

## Transverse momentum broadening and collinear radiation at NLO in the $\mathcal{N}=4$ SYM plasma

---

Jacopo Ghiglieri,<sup>1</sup> HyungJoo Kim<sup>1,2</sup>

<sup>1</sup>*Theoretical Physics Department, CERN,  
CH-1211 Geneva 23, Switzerland*

<sup>2</sup>*Department of Physics, Yonsei University,  
50 Yonsei-ro, Seoul 03722, Korea*

*E-mail:* [jacopo.ghiglieri@cern.ch](mailto:jacopo.ghiglieri@cern.ch), [hyungjoo.kim@cern.ch](mailto:hyungjoo.kim@cern.ch)

**ABSTRACT:** We compute  $\mathcal{O}(g)$  NLO corrections to the transverse scattering kernel and transverse momentum broadening coefficient  $\hat{q}$  of weakly-coupled  $\mathcal{N} = 4$  SYM. Based on this, we also compute NLO correction to the collinear splitting rates. For  $\hat{q}$  we find that the NLO/LO ratio is similar to the QCD one, with large NLO corrections. This is contrasted by our findings for the collinear splitting rate, which show a much better convergence in SYM than in QCD, providing further support to earlier expectations that NLO corrections have signs and relative magnitudes controlled by the specifics of the theory. We also compare the ratio of  $\hat{q}$  in QCD and in  $\mathcal{N} = 4$  theory to strong coupling expectations.

**KEYWORDS:** Thermal Field Theory, Higher-order corrections, Supersymmetric gauge theory

---

## Contents

<b>1</b>	<b>Introduction</b>	<b>1</b>
<b>2</b>	<b>Theoretical setup</b>	<b>3</b>
<b>3</b>	<b>The collision kernel at NLO</b>	<b>5</b>
<b>4</b>	<b>The transverse momentum broadening coefficient at NLO</b>	<b>10</b>
4.1	Comparisons with AdS/CFT results	16
<b>5</b>	<b>Collinear radiation rate</b>	<b>18</b>
<b>6</b>	<b>Summary and conclusions</b>	<b>21</b>
<b>A</b>	<b>Feynman Rules of ESYM</b>	<b>23</b>
<b>B</b>	<b>Scalar contributions to the one-loop diagrams in Fig. 3</b>	<b>24</b>

---

## 1 Introduction

The characterization of the QCD medium produced in heavy ion collisions, and possibly also in smaller systems (proton-nucleus and high-multiplicity proton-proton collisions) proceeds through the complementary study of bulk properties and hard probes. The AdS/CFT correspondence [1–3] has been widely applied in both cases over the past 20 years (see [4] for a review), providing great qualitative insight on the strong-coupling regime of QCD, in particular for quantities such as the specific shear viscosity  $\eta/s$  [5–7], which are not directly accessible from lattice QCD without arduous analytical continuations (see [8] for a review).

In its standard form, the AdS/CFT correspondence conjectures a duality between conformal  $\mathcal{N} = 4$  Super-Yang-Mills (SYM) theory in  $D = 4$  spacetime dimensions and type-IIB string theory in  $AdS_5 \times S^5$ . At large values of the 't Hooft coupling  $\lambda$  and for large numbers of colors  $N_c$ , calculations on the holographic side become accessible 5D gravity computations; a finite-temperature system in the CFT corresponds to a black hole in AdS. This has led to the aforementioned wealth of computations of quantities of interest for heavy-ion physics at strong coupling. If one wants more than a qualitative insight when applying strong-coupling, holographic results to the QCD medium, one needs to understand a double extrapolation: from  $\mathcal{N} = 4$  SYM to QCD, and from  $\lambda \rightarrow \infty$  to the regime of “intermediate” couplings one expects for heavy ion collisions, such as  $\alpha_s \equiv g^2/(4\pi) \approx 0.3$ ,  $\lambda \equiv g^2 N_c \approx 10$ .

To this end, an important step forward would be the understanding of thermal  $\mathcal{N} = 4$  SYM at all values of  $\lambda$ . On the large coupling side, for many quantities, such as the photon rate [9] or the viscosity, the first corrections in the inverse coupling in AdS have been computed, in [10] and [11–14] respectively. At weak coupling, calculations can be performed directly on the CFT side, using the tools of finite-temperature perturbation theory. Leading-order (LO) results for the photon rate and the viscosity have been presented in [9] and [15], in both cases following the path set by previous perturbative QCD (pQCD) calculations, [16] and [17, 18] respectively. Once  $\mathcal{N} = 4$  SYM results in the two regimes are available, one can try to extrapolate from both sides towards the interesting intermediate region.

Clearly, this exercise requires the best possible knowledge on both sides. At weak coupling, calculations of transport coefficients and of dynamical quantities like the photon rate are notoriously difficult, requiring different sets of resummations already at LO. Over the past decade, a new understanding of the analytical properties of thermal amplitudes at light-like separations has emerged [19] (see [20] for a more pedagogic presentation). Owing to this development, next-to-leading order (NLO) pQCD calculations of the photon rate [21] and of transport coefficients [22, 23] have recently appeared. Their extension to  $\mathcal{N} = 4$  SYM would thus lead to an “extrapolation game”, as we have sketched before, with the first corrections in both regimes and thus a first estimate of the uncertainty. Furthermore, one could compare the QCD and SYM NLO weak-coupling results, to get a better understanding on how to deal with the different type and number of degrees of freedom when applying holographic results.

Motivated by this, in this paper we investigate the *jet quenching parameter*  $\hat{q}$  at NLO in  $\mathcal{N} = 4$  SYM. Also known as the transverse momentum broadening coefficient,  $\hat{q} \equiv \langle p_{\perp}^2 \rangle / L$  describes how much transverse momentum  $p_{\perp}$  is picked up per length  $L$  by a highly energetic parton propagating through a plasma. It is thus extremely important for the physics of jet quenching (see [24–30]), where it is a parameter in many theoretical models of medium-modified radiation from the hard partons constituting the jet (see [31] for a comparison with/extraction from data and [32] for a theoretical comparison of the models). In this paper, we will study  $\hat{q}$  and the related *transverse scattering kernel* (or collision kernel)  $\mathcal{C}(q_{\perp})$  at NLO. Both quantities are known in the strong-coupling limit [33–35], together with part of the first corrections in the inverse coupling [36] (see also [37, 38] for related strong-coupling calculations for massive probes). In weak-coupling QCD, leading- and next-to-leading results have been obtained in [39, 40] and [19] respectively. Hence, we shall be in the position to compare both weak-coupling results in the two different theories and weak and strong coupling within  $\mathcal{N} = 4$  SYM.

Furthermore,  $\hat{q}$  and  $\mathcal{C}(q_{\perp})$  are two of the main ingredients in many other perturbative calculations: the former has been found in [22] to be the main driver of the large NLO corrections to the transport coefficients, while the latter determines the NLO correction to *collinear radiation*, which is an important ingredient both in the kinetic theory used to determine transport coefficients [41, 42] and in the thermal photon rate. Hence, as a first application of our NLO results, we also compute the collinear radiation rate, or collinear splitting rate, at NLO, to study its sensitivity to the different quasiparticle degrees of

freedom in QCD and SYM.

At the technical level, the calculation of  $\hat{q}$  and  $\mathcal{C}(q_\perp)$  can be separated into soft ( $gT$ -scale) and hard ( $T$ -scale) contributions. At leading-order the soft contribution is known [9, 39], while in the hard region we will determine the contribution from the SYM scalars. At NLO only the soft scale enters: our calculation requires the evaluation of soft one-loop corrections to the Wilson loop from which these are defined [35, 43]. The aforementioned new understanding of the analytical properties of thermal amplitudes leads in this case to a great simplification, as the problem can be mapped to a much simpler one within the dimensionally-reduced Euclidean theory. In the case of QCD this is Electrostatic QCD (EQCD) [44–48], while in the case of SYM this is usually called ESYM [49], whose kinetic term was written down in [49–51]. We will thus need to analyze in detail the contribution of the scalars of  $\mathcal{N} = 4$  theory to ESYM in general and to our observables in particular (fermions are not an explicit degree of freedom of the dimensionally-reduced theories).

Finally, we also remark that the transverse scattering kernel of the electroweak (EW) theory is similarly a very important ingredient in determinations of the collinear radiation rate within that theory, which is of relevance for applications such as the collinear thermal production of right-handed neutrinos [52, 53]. Our NLO calculation, with its in-depth analysis of the scalar contribution, will thus be very helpful in extending the EW calculation towards NLO, whose necessity has been pointed out in [54] and which requires the evaluation of the contribution of the Higgs scalar doublet.

The paper is organized as follows: in Sec. 2 we review the theoretical setup and definitions. Sec. 3 is devoted to the computation of  $\mathcal{C}(q_\perp)$  at NLO in ESYM, while in Sec. 4 we discuss  $\hat{q}$  at NLO and its relation with the strong-coupling and QCD results. In Sec. 5 we apply our results to the collinear splitting rate and we draw our conclusions in Sec. 6. Technical details are to be found in the Appendices.

## 2 Theoretical setup

The collision kernel  $\mathcal{C}(q_\perp)$  describing the evolution of the transverse momentum of a very hard particle with momentum  $\mathbf{p}$  and energy  $E \approx p$ , with  $E \gg T$ , is defined as

$$\mathcal{C}(q_\perp) \equiv \lim_{p \rightarrow \infty} (2\pi)^2 \frac{d\Gamma_{\text{scatt}}(\mathbf{p}, \mathbf{p} + \mathbf{q}_\perp)}{d^2q_\perp}, \quad (2.1)$$

where  $q_\perp$  is the transverse momentum ( $\mathbf{q}_\perp \cdot \mathbf{p} = 0$ ) acquired in the scattering.<sup>1</sup> The collision kernel can be defined in a field-theoretical manner using the Wilson loop in the  $(x^+, x_\perp)$  plane [35, 43] sketched in Fig. 1. Here we use light-cone coordinates defined as  $p^- \equiv p^0 - p^z$ ,  $p^+ \equiv \frac{p^0 + p^z}{2}$ , and  $\mathbf{p}_\perp = (p^x, p^y)$  for convenience. The Wilson loop is then written explicitly as

$$\langle W(x_\perp, L) \rangle = \frac{1}{d_R} \left\langle \text{Tr} \tilde{U}(0, \mathbf{x}_\perp; 0) U(0, L; \mathbf{x}_\perp) \tilde{U}(\mathbf{x}_\perp, 0; L) U(L, 0; 0) \right\rangle, \quad (2.2)$$

---

<sup>1</sup>In our convention the metric is  $g_{\mu\nu} = (-+++)$ ,  $P = (p^0, \mathbf{p})$  is a four-vector, with  $\mathbf{p}$  the three-vector with modulus  $p$ .

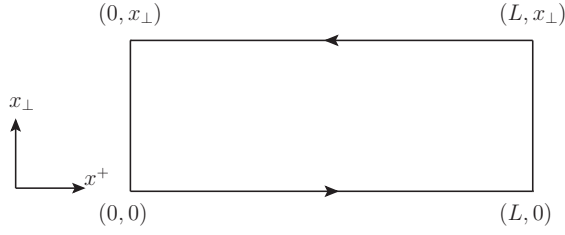


**Figure 1.** Wilson loop  $W(x_\perp, L)$  leading to  $\mathcal{C}'(x_\perp)$ .

where the Wilson lines are defined as<sup>2</sup>

$$\begin{aligned}
 U(a, b; x_\perp) &= P \exp \left( -ig \int_b^a dx^+ A^-(x^+, x^- = 0, x_\perp) \right), \\
 \tilde{U}(\mathbf{a}, \mathbf{b}; x^+) &= P \exp \left( -ig \int_0^1 ds (\mathbf{a} - \mathbf{b}) \cdot \mathbf{A}_\perp(x^+, x^- = 0, x_\perp = s(\mathbf{a} - \mathbf{b})) \right). \quad (2.3)
 \end{aligned}$$

The trace runs over the color degrees of freedom, with the source taken in representation  $R$  with  $d_R$  its dimension. In QCD, hard quarks will be described by the fundamental Wilson loop  $R = F$  and hard gluons by the adjoint one,  $R = A$ . In  $\mathcal{N} = 4$  SYM all d.o.f.s transform in the adjoint.  $\langle \dots \rangle$  denotes a thermal average. Finally, the operators should be intended ordered such that fields on the backward-propagating Wilson line  $U(0, L; \mathbf{x}_\perp)$  come always to the left of those in the forward-propagating one, as they are associated with the conjugate amplitude and amplitude respectively or, in the Schwinger-Keldysh language, the anti-time ordered and time-ordered parts of the contour [35, 43].

$\mathcal{C}(q_\perp)$  can then be obtained from this Wilson loop in the large  $L$  limit as

$$\mathcal{C}'(x_\perp) = - \lim_{L \rightarrow \infty} \frac{1}{L} \ln \langle W(x_\perp, L) \rangle \quad (2.4)$$

where  $\mathcal{C}'(x_\perp)$  is the collision kernel in impact-parameter space, i.e.

$$\mathcal{C}'(x_\perp) \equiv \int \frac{d^2 q_\perp}{(2\pi)^2} (1 - e^{i\mathbf{q}_\perp \cdot \mathbf{x}_\perp}) \mathcal{C}(q_\perp). \quad (2.5)$$

We use the  $\mathcal{C}'(x_\perp)$  notation as a reminder that  $\mathcal{C}'(x_\perp)$  is *not* the Fourier transform of  $\mathcal{C}(q_\perp)$ .<sup>3</sup>

Finally, the transverse momentum broadening coefficient  $\hat{q}$  can be obtained as the second moment of  $\mathcal{C}(q_\perp)$ , i.e.

$$\hat{q} \equiv \int_0^{q_{\max}} \frac{d^2 q_\perp}{(2\pi)^2} q_\perp^2 \mathcal{C}(q_\perp), \quad (2.7)$$

<sup>2</sup>This definition is valid both in QCD and in  $\mathcal{N} = 4$  SYM.

<sup>3</sup>Equally importantly, we remark that  $\mathcal{C}(q_\perp)$  is *not* the Fourier transform of  $\langle W(x_\perp, L) \rangle$ . That quantity is instead called  $P(q_\perp)$ , the probability for the hard parton to pick up a certain transverse momentum  $q_\perp$ . It reads [35, 43]

$$P(q_\perp) \equiv \int d^2 x_\perp e^{-i\mathbf{q}_\perp \cdot \mathbf{x}_\perp} \langle W(x_\perp, L) \rangle. \quad (2.6)$$

where  $q_{\max}$  is a process-dependent UV regulator that is in general needed at weak coupling. As we are interested in hard particles of energy/momentum  $E \gg T$ , we shall take  $q_{\max} \gg T$  as well.<sup>4</sup> Finally, the eikonal propagation of the hard parton, which gives rise to the Wilson loop above, is only valid insofar the transferred momentum  $q_{\perp}$  does not affect the hard parton's. Hence, we must also require  $E \gg q_{\max}$ .

At leading order the scattering kernel and  $\hat{q}$  receive contributions from gluon-mediated elastic scatterings off the medium constituents [19, 40]. This is true in any gauge theory. Since the Coulomb scattering matrix element squared is proportional to  $t^{-2}$ , we expect a  $1/q_{\perp}^4$  behavior in the scattering kernel. Thus scatterings with  $q_{\perp} \sim T$  and softer ones with  $q_{\perp} \sim gT$  contribute at the same order (up to logarithms) to Eq. (2.7).  $gT$  is the scale at which collective effects such as Debye screening and Landau damping appear in a weakly-coupled plasma; we call it the *soft scale*. We will call  $T$  the *hard scale*, with the understanding that the energy/momentum  $E \gg T$  of the probe is called *very hard*. It is convenient to introduce a regulator  $q^*$ , with  $gT \ll q^* \ll T$ , to separate the soft and hard contributions, i.e.

$$\hat{q} = \int_0^{q^*} \frac{d^2 q_{\perp}}{(2\pi)^2} q_{\perp}^2 \mathcal{C}_{\text{soft}}(q_{\perp}) + \int_{q^*}^{q_{\max}} \frac{d^2 q_{\perp}}{(2\pi)^2} q_{\perp}^2 \mathcal{C}_{\text{hard}}(q_{\perp}), \quad (2.8)$$

In perturbative Thermal Field Theory, soft bosons in equilibrium are highly occupied, since the Bose–Einstein distribution  $n_B(q^0) = (e^{q^0/T} - 1)^{-1}$  becomes approximately  $T/q^0 \sim 1/g$  there. Hence, soft-boson loops are not suppressed by the usual factor of  $g^2$ , which characterizes hard (or zero-temperature) loops, but by a single factor of  $g$ . Therefore, NLO corrections to  $\hat{q}$  come from one-loop bosonic diagrams at  $q_{\perp} \sim gT$ . In QCD these are only gauge (gluon and ghost) loops, whereas in  $\mathcal{N} = 4$  SYM there is also a scalar contribution. In either case, the analytical properties stemming from light-cone causality allow these contributions to  $\mathcal{C}_{\text{soft}}(q_{\perp})$  (and thereupon  $\hat{q}$ ) to be computed within the simpler dimensionally-reduced theory, as we show in the next section. We will then discuss  $\hat{q}$  and  $\mathcal{C}_{\text{hard}}(q_{\perp})$  in Sec. 4. Finally, we remark that, by the same arguments on the Bose–Einstein distribution, the *ultrasoft* (or magnetic) scale  $g^2T$  has no loop suppression factor and is thus non-perturbative [56]. However, its contribution to  $\hat{q}$  is suppressed by  $g^2$  with respect to the LO [19, 43, 55, 57] and is thus beyond our  $\mathcal{O}(g)$  accuracy. Knowledge of  $\mathcal{C}(q_{\perp} \sim g^2T)$  is also not needed, as it does not contribute to the collinear radiation rates at LO or NLO. As remarked in [43, 57, 58], both can be obtained within the Euclidean framework using non-perturbative methods.

### 3 The collision kernel at NLO

In principle, a one-loop, soft-loop calculation would require a thorough analytical and numerical effort in the Hard Thermal Loop (HTL) effective theory [59, 60] (see [61] for the complete HTL structure of  $\mathcal{N} = 4$  SYM). However, as shown by Caron-Huot [19] in the

---

<sup>4</sup>Our definition, Eq. (2.7), is slightly different from the one in [35, 43], which involves the second moment of  $P(q_{\perp})$ , defined in Footnote 3. However, as shown in [55], the two different definitions give rise to the same result.

context of the NLO calculation of  $\hat{q}$  in QCD, light-cone causality makes correlators such as Eq. (2.2) dramatically simpler, leading to a Euclidean formulation. Indeed, he has shown that the soft contribution to many space-like separated correlators can be mapped to a dimensionally reduced Euclidean theory, which integrates out all the non-zero Matsubara modes. Based on that, he proceeded to determine the one-loop, soft-loop contribution to Eq. (2.2) with EQCD.

We can apply the same strategy to  $\mathcal{N} = 4$  SYM theory. Electrostatic SYM [49–51] is a dimensionally-reduced 3D Euclidean theory of  $\mathcal{N} = 4$  SYM for the soft ( $gT$ ) scale physics. We now use this effective theory to calculate the  $\mathcal{O}(g)$  contribution to the collision kernel and to the transverse momentum broadening coefficient of the weakly coupled  $\mathcal{N} = 4$  SYM plasma. Keeping only the operators that are needed for this calculation, the Lagrangian of ESYM reads

$$\begin{aligned} \mathcal{L}_{ESYM} = & \frac{1}{4} F_{ij}^a F_{ij}^a + \frac{1}{2} (D_i A_0)^a (D_i A_0)^a + \frac{1}{2} (D_i \phi_I)^a (D_i \phi_I)^a + \frac{1}{2} m_E^2 A_0^a A_0^a + \frac{1}{2} m_S^2 \phi_I^a \phi_I^a \\ & + \frac{1}{2} \lambda_{ES} f^{abc} f^{ade} \phi_I^b A_0^c \phi_I^d A_0^e + \dots, \end{aligned} \quad (3.1)$$

where  $F_{ij}^a = \partial_i A_j^a - \partial_j A_i^a + g_E f^{abc} A_i^b A_j^c$  and  $(D_i \Phi)^a = \partial_i \Phi^a + g_E f^{abc} A_i^b \Phi^c$  for any  $SU(N_c)$  adjoint bosonic field  $\Phi^a \in \{A_i^a, A_0^a, \phi_I^a\}$ .  $I \in 1, \dots, n_S$  spans the  $n_S = 6$  real scalars of  $\mathcal{N} = 4$  SYM. The interaction term on the second line is new to this work, as the references in the literature focused on the kinetic terms only. These reflect how, under dimensional reduction, the spatial components  $A_i^a$  remain gauge fields, while  $A_0^a$  becomes a massive, *electrostatic* adjoint scalar field and the scalars  $\phi_I^a$  become massive as well, with masses  $m_E$  and  $m_S$  respectively. Fermions are fully integrated out during dimensional reduction and only contribute to the Wilson coefficients, such as these masses. At leading order, the matching between  $\mathcal{N} = 4$  SYM and ESYM yields [49–51]

$$g_E^2 = g^2 T, \quad \lambda_{ES} = g^2 T, \quad (3.2)$$

$$m_E^2 = \frac{C_A g^2 T^2}{3} \left(1 + \frac{n_S}{2} + \frac{n_f}{2}\right) = 2\lambda T^2, \quad m_S^2 = \frac{C_A g^2 T^2}{6} \left(1 + \frac{n_S}{2} + \frac{n_f}{2}\right) = \lambda T^2, \quad (3.3)$$

where  $g_E$  is the dimensionful coupling of ESYM,  $g$  is the coupling of  $\mathcal{N} = 4$  SYM,  $C_A = N_c$  the quadratic Casimir of the adjoint representation and  $\lambda \equiv g^2 N_c$  is the 't Hooft coupling. In our conventions  $n_f = 4$  counts the number of Weyl fermion species of  $\mathcal{N} = 4$  SYM. We note that the electrostatic mass  $m_E$  equals at leading order the Debye mass; we shall use both terms in the following. Our graphical conventions for scalars and gauge fields, as well as the Feynman rules derived from Eq. (3.1), are illustrated in App. A.

As we explained, the calculation of this Wilson loop is reduced to the calculation using ESYM. In any non-singular gauge the transverse Wilson lines become irrelevant in the large- $L$  limit. There, the LO contribution from the soft region comes from the single-gluon exchange diagrams shown in Fig. 2. We exploit the manifest gauge invariance of the definition in Eq. (2.2) to compute in Feynman gauge, as shown in App. A and B. A straightforward evaluation leads then to [9, 39]

$$c_{\text{soft}}^{(\text{LO})}(q_\perp) = g^2 C_R T \left[ \frac{1}{q_\perp^2} - \frac{1}{q_\perp^2 + m_E^2} \right] = \frac{g^2 C_R T m_E^2}{q_\perp^2 (q_\perp^2 + m_E^2)}, \quad (3.4)$$



**Figure 2.** Diagrams contributing to  $\mathcal{C}_{\text{soft}}(q_{\perp})$  at LO. As shown in detail in App. A, curly lines are the  $A^i$  gauge fields, solid lines are the electrostatic scalars  $A^0$ . The parallel lines represent the Wilson line along the  $x^+$  direction separated by  $x_{\perp}$ .

where the first term in square brackets is the gauge propagator  $G^{zz}$  and the second term the massive, electrostatic propagator  $G^{00}$ . Even though in  $\mathcal{N} = 4$  SYM all sources are adjoint, we prefer for now to keep  $C_R$  unassigned, so that we can keep the connection to the QCD calculation more transparent and at the same time keep our results more general, so that they can be more easily adapted to the electroweak theory as well, with its different group theory factors.

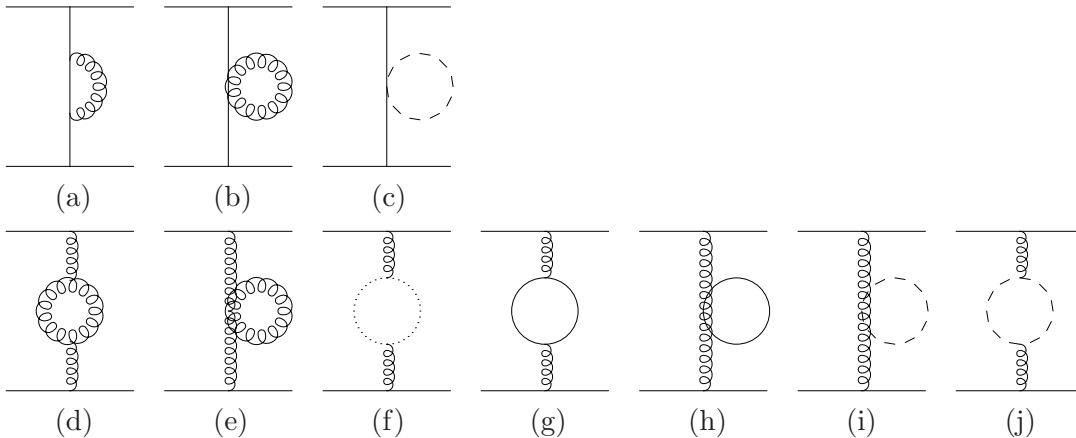


**Figure 3.** One-loop self-energy diagrams contributing to  $\delta\mathcal{C}(q_{\perp})$ . In addition to the conventions of Fig. 2, dotted lines are ghosts and dashed lines are the scalars  $\phi_I$ .

The NLO soft scattering kernel can be written symbolically as

$$\mathcal{C}_{\text{soft}}^{(\text{NLO})}(q_{\perp}) \equiv \mathcal{C}_{\text{soft}}^{(\text{LO})}(q_{\perp}) + \delta\mathcal{C}(q_{\perp}). \quad (3.5)$$

The NLO contributions in  $\delta\mathcal{C}(q_{\perp})$  can come from the soft one-loop self-energy insertion into the LO diagrams and from “multi-gluon exchanges” (e.g. two single-gluon exchanges, three gluon vertex). In Fig. 3, we draw the one-loop self energy diagrams contributing to NLO. Diagrams on the first line are one-loop self energy diagrams of the  $G^{00}$  propagator and those on the second line are for the  $G^{zz}$  propagator. NLO corrections from the scalar field  $\phi_I^a$  can only contribute to these self-energy diagrams. The “multi-gluon-exchange” diagrams, such as those drawn in Fig. 4, have no NLO corrections from the scalar fields and are thus equivalent to the QCD case calculated in [19].



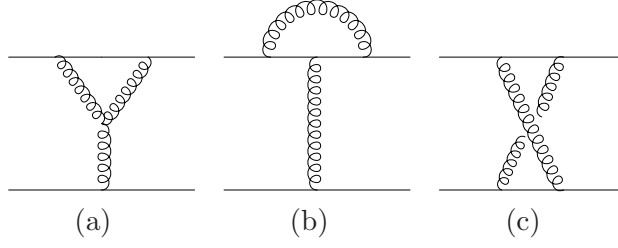


**Figure 4.** Some “multi-gluon-exchange” diagrams contributing to NLO.

Hence, diagrams (c), (i) and (j) in Fig. 3 are what we need to compute directly within ESYM. We refer to App. B for the detailed evaluation, whose final result reads

$$\frac{\delta\mathcal{C}_{\text{scalar}}(q_{\perp})}{g^4 T^2 C_R C_A} = -\frac{3m_S}{2\pi(q_{\perp}^2 + m_E^2)^2} + 6\frac{m_S - \frac{q_{\perp}^2 + 4m_S^2}{2q_{\perp}} \tan^{-1}(q_{\perp}/2m_S)}{8\pi q_{\perp}^4}, \quad (3.6)$$

where the first term comes from diagram (c) and the second from (i) and (j). This can be added to the QCD contribution in [19] to give

$$\begin{aligned} \frac{\delta\mathcal{C}(q_{\perp})}{g^4 T^2 C_R C_A} &= \frac{7}{32q_{\perp}^3} + \frac{m_E}{4\pi(q_{\perp}^2 + m_E^2)} \left( \frac{3}{q_{\perp}^2 + 4m_E^2} - \frac{2}{q_{\perp}^2 + m_E^2} - \frac{1}{q_{\perp}^2} \right) \\ &+ \frac{-m_E - 2\frac{q_{\perp}^2 - m_E^2}{q_{\perp}} \tan^{-1}\left(\frac{q_{\perp}}{m_E}\right)}{4\pi(q_{\perp}^2 + m_E^2)^2} + \frac{m_E - \frac{q_{\perp}^2 + 4m_E^2}{2q_{\perp}} \tan^{-1}\left(\frac{q_{\perp}}{2m_E}\right)}{8\pi q_{\perp}^4} \\ &- \frac{\tan^{-1}\left(\frac{q_{\perp}}{m_E}\right)}{2\pi q_{\perp}(q_{\perp}^2 + m_E^2)} + \frac{\tan^{-1}\left(\frac{q_{\perp}}{2m_E}\right)}{2\pi q_{\perp}^3} \\ &- \frac{3m_S}{2\pi(q_{\perp}^2 + m_E^2)^2} + 6\frac{m_S - \frac{q_{\perp}^2 + 4m_S^2}{2q_{\perp}} \tan^{-1}\left(\frac{q_{\perp}}{2m_S}\right)}{8\pi q_{\perp}^4}. \end{aligned} \quad (3.7)$$

This expression is well suited for the evaluation of  $\hat{q}$  in Eqs. (2.7) and (2.8). However, the NLO collinear radiation rate we shall present in Sec. 5 is most easily evaluated from the impact-parameter space expression, Eq. (2.5). To perform the needed Fourier transform, we follow the same strategy used in [21], that is to choose  $\mathbf{x}_{\perp} = (x_{\perp}, 0)$ , perform the integration for  $q_y$  first and then for  $q_x$ , using contour techniques. When the latter cannot be done analytically, it has in any case become an integration with a (real) exponential kernel rather than an oscillatory one, thus better suited for numerical integration. Schematically, one has

$$\mathcal{C}'(x_{\perp}) \equiv \int \frac{d^2 q_{\perp}}{(2\pi)^2} (1 - e^{i\mathbf{q}_{\perp} \cdot \mathbf{x}_{\perp}}) \mathcal{C}(q_{\perp}) = \int_{-\infty}^{\infty} \frac{dq_x}{2\pi} (1 - e^{ix_{\perp} q_x}) \int_{-\infty}^{\infty} \frac{dq_y}{2\pi} \mathcal{C}(q_{\perp}). \quad (3.8)$$

At LO this becomes straightforwardly

$$\mathcal{C}'^{(\text{LO})}(x_{\perp}) = \frac{g^2 C_R T}{2\pi} (K_0(x_{\perp} m_E) + \gamma_E + \ln(x_{\perp} m_E/2)), \quad (3.9)$$

where this is intended to be the soft contribution, i.e. valid at distances  $x_\perp \sim 1/(gT)$ . At NLO we obtain  $\mathcal{C}'^{(\text{NLO})}(x_\perp) = \mathcal{C}'^{(\text{LO})}(x_\perp) + \delta\mathcal{C}'(x_\perp)$ , with the NLO correction given by

$$\begin{aligned}
& \frac{m_E \delta\mathcal{C}'(x_\perp)}{g^4 T^2 C_R C_A} \\
&= \frac{3m_S}{8\pi^2 m_E} (x_\perp m_E K_1(x_\perp m_E) - 1) - \frac{m_E}{16\pi^2 m_S} \int_0^\infty \frac{dz}{z^4} (1 - e^{-x_\perp m_S z}) (z^3 - (z^2 - 4)^{3/2} \theta(z - 2)) \\
&\quad - \frac{1}{8\pi^2} \left\{ \frac{x_\perp m_E K_1(x_\perp m_E) + 3 - 4e^{-x_\perp m_E}}{2} + \int_1^\infty dz (e^{-x_\perp m_E} - e^{-x_\perp m_E z}) \frac{\ln \frac{z^2}{z^2 - 1}}{(z^2 - 1)^{3/2}} \right\} \\
&\quad - \frac{1}{96\pi^2} \int_0^\infty \frac{dz}{z^4} (1 - e^{-x_\perp m_E z}) (z^3 - (z^2 - 4)^{3/2} \theta(z - 2)) + \frac{7x_\perp m_E}{64\pi} - \frac{1}{32} \\
&\quad + \frac{1}{8\pi^2} \int_1^\infty dz \frac{e^{-x_\perp m_E z} \ln \frac{z^2}{z^2 - 1}}{\sqrt{z^2 - 1}} + \frac{1}{8\pi^2} \int_0^\infty \frac{dz}{z^2} (1 - e^{-x_\perp m_E z}) (z - \theta(z - 2) \sqrt{z^2 - 4}) \\
&\quad + \frac{1}{8\pi^2} (K_0(2x_\perp m_E) - 2K_0(x_\perp m_E) + \ln \frac{4}{x_\perp m_E} - \gamma_E + x_\perp m_E K_1(x_\perp m_E) - 1), \quad (3.10)
\end{aligned}$$

where we have written the SYM-specific terms originating from soft scalar loops on the first line. All other terms are shared with the QCD case in [21].

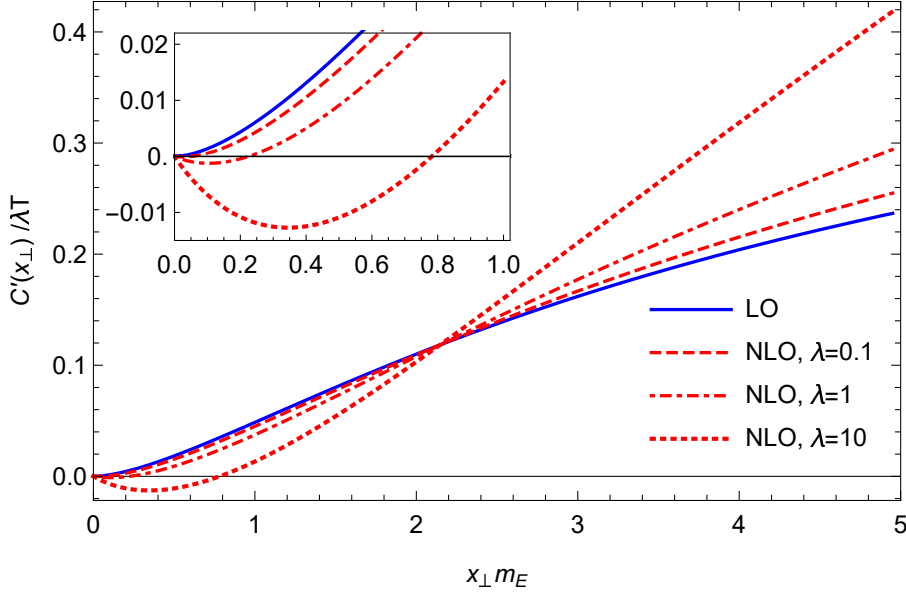


**Figure 5.**  $\mathcal{C}'(x_\perp)/\lambda T$  as a function of  $x_\perp m_E$ . The solid blue line is the LO expression, Eq. (3.9), while the red lines are given by the sum of Eqs. (3.9) and (3.10).

While we defer plots and considerations on the size of the NLO momentum-space corrections to the next section, we plot in Fig. 5 the LO and NLO impact-parameter space kernels for three different choices of coupling ranging from small to intermediate. As the plot shows, the NLO collision kernel becomes negative close to the origin. That is quite obviously an UV ( $q_\perp \gg gT$ ) effect: we will comment more on this in the next section. In the validity region of the soft calculation,  $x_\perp m_E \sim 1$ , the NLO curve can be either below or above the LO one, while at the opposite asymptote at large  $x_\perp$  it is larger.

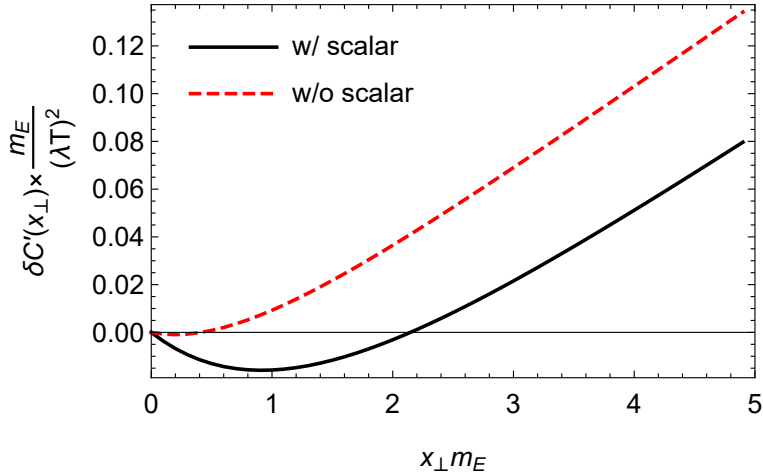


**Figure 6.**  $\delta\mathcal{C}'(x_\perp) \times m_E/(\lambda T)^2$  as a function of  $x_\perp m_E$ . The solid black line is Eq. (3.10), while the dashed red line is the QCD contribution only, without the scalar loop contribution.

To show the impact of the new scalar contribution that is unique to SYM, in Fig. 6 we plot the NLO correction  $\delta\mathcal{C}'(x_\perp)$  with and without it, that is, in SYM and in QCD. The figure clearly shows how the SYM scalar contribution magnifies the negative dip already present in QCD, where it was noted in [21]. As we shall comment later, this negative dip will also have a marked impact on the collinear radiation rate.

#### 4 The transverse momentum broadening coefficient at NLO

As we illustrated in Sec. 2, the transverse momentum broadening coefficient  $\hat{q}$  is given by the second moment of the collision kernel, as shown in Eq. (2.7). We then introduced  $q^*$  as an intermediate regulator to separate the soft and hard contribution in Eq. (2.8). In the previous section we have reviewed the LO determination of  $\mathcal{C}_{\text{soft}}(q_\perp)$  and computed its NLO correction. The soft contribution to  $\hat{q}$  at LO and NLO follow from Eqs. (3.4) and (3.7) and are given by

$$\hat{q}_{\text{soft}}^{(\text{LO})} = \frac{g^2 T C_R m_E^2}{2\pi} \log\left(\frac{q^*}{m_E}\right), \quad (4.1)$$

$$\delta\hat{q} = \frac{g^4 T^2 C_R C_A}{2\pi} \left[ -\frac{q^*}{4} + m_E \frac{3\pi^2 + 10 - 4\log 2}{16\pi} + m_S \frac{3(1 - \log 2)}{4\pi} \right], \quad (4.2)$$

where we have used the fact that  $\log \frac{m_E}{m_S} = \frac{1}{2} \log 2$  at leading order. The  $m_S$ -proportional contribution in Eq. (4.2) is the SYM-specific one arising from scalars. We see that, while the LO contribution is logarithmically sensitive to  $q^*$ , as anticipated, the NLO contribution presents a linear term in the cutoff and a finite contribution (where  $q^*$  has been taken to infinity in its evaluation). The linear term is related to the negative dip in  $\delta\mathcal{C}'(x_\perp)$  at small  $x_\perp$  observed previously: as we shall show later, it will cancel against the hard contribution.

Eqs. (4.1) and (4.2) are already enough to determine  $\hat{q}$  if  $gT \ll q_{\text{max}} \ll T$ , as is the case when dealing with diffusion processes in the Landau expansion of the collision operator

in the investigation of transport coefficients [22] or of high-energy partons [42]. However, in the interest of generality, we have fixed  $q_{\max} \gg T$ , as appropriate for the momentum broadening of a very hard parton, and we thus need to deal with the hard contribution from the scale  $T$ ,  $\mathcal{C}_{\text{hard}}(q_{\perp})$ .

As we have mentioned before, the leading-order contribution comes from elastic  $2 \leftrightarrow 2$  scatterings with medium constituents. In the soft sector these get Landau-damped, leading to Eq. (3.4), whereas in the hard sector one can evaluate the matrix elements without any resummation and convolute them with the statistical factors for the medium scatterers. In the QCD case this gives [19, 40]

$$\mathcal{C}_{\text{hard}}^{\text{QCD}}(q_{\perp}) = \frac{g^4 C_R}{q_{\perp}^4} \int \frac{d^3 p}{(2\pi)^3} \frac{p - p_z}{p} \left[ 2C_A n_B(p)(1 + n_B(p')) + 4N_f T_F n_F(p)(1 - n_F(p')) \right], \quad (4.3)$$

where  $p' = p + \frac{q_{\perp}^2 + 2q_{\perp} \cdot p}{2(p - p_z)}$ ,  $n_F(p) = (e^{p/T} + 1)^{-1}$  is the Fermi–Dirac distribution,  $T_F = 1/2$  for the  $N_f$  fundamental Dirac fermions of QCD, not to be confused with  $n_f = 4$ , which counts the number of Weyl fermions of  $\mathcal{N} = 4$  SYM. We refer to [40] for details on the accurate numerical evaluation of this expression.

Eq. (4.3) is transparently given by the sum of a contribution from scattering off gluons, proportional to  $C_A n_B(1 + n_B)$ , and of a contribution from scattering off quarks and antiquarks, proportional to  $N_f T_F n_F(1 - n_F)$ . In principle the matrix elements for these scatterings, and for those involving external and intermediate scalars in  $\mathcal{N} = 4$  SYM, differ from each other (see [15, 61] for a complete list). However, as noted in [19, 40, 62], when the external energy  $E$  of the very hard probe becomes much larger than  $T$ , the Mandelstam invariants  $s \approx ET$  and  $t = -q_{\perp}^2 \sim T^2$  become hierarchically separated, with  $s \gg |t|$ . In this limit the matrix elements simplify greatly and acquire a spin-independent, universal eikonal form proportional to  $s^2/t^2$ , which explains why the gluon and quark contributions in Eq. (4.3) differ only in the statistical functions and group-theoretical factors. In order to obtain the  $\mathcal{N} = 4$  SYM hard contribution we thus have to adjust the number and representation of the scatterers in Eq. (4.3). In the bosonic sector, the  $2C_A$  of QCD has to become  $(2 + 6)C_A$ , to account for the two spin states of the gluon and the six real scalars. In the fermionic sector  $4N_f T_F$  has to become  $2n_f C_A$  to account for the  $n_f$  Weyl fermions, which contribute each half as much as a Dirac fermion, and which transform in the adjoint representation,  $T_A = C_A$ . We then have

$$\mathcal{C}_{\text{hard}}^{\text{SYM}}(q_{\perp}) = \frac{g^4 C_R}{q_{\perp}^4} \int \frac{d^3 p}{(2\pi)^3} \frac{p - p_z}{p} \left[ 8C_A n_B(p)(1 + n_B(p')) + 2n_f C_A n_F(p)(1 - n_F(p')) \right]. \quad (4.4)$$

The integration of Eq. (4.4) and its insertion in Eq. (2.8) give the hard contribution to  $\hat{q}$  in  $\mathcal{N} = 4$  SYM, which reads

$$\begin{aligned} \frac{\hat{q}_{\text{hard}}}{g^4 C_R T^3} &= \frac{4C_A}{6\pi} \left[ \log\left(\frac{T}{q^*}\right) + \frac{\zeta(3)}{\zeta(2)} \log\left(\frac{q_{\max}}{T}\right) - 0.0688854926766592 \dots + \frac{3}{16} \frac{q^*}{T} \right] \\ &+ \frac{n_f C_A}{12\pi} \left[ \log\left(\frac{T}{q^*}\right) + \frac{3}{2} \frac{\zeta(3)}{\zeta(2)} \log\left(\frac{q_{\max}}{T}\right) - 0.072856349715786 \dots \right] + \mathcal{O}\left(\frac{q_*^2}{T^2}\right), \end{aligned} \quad (4.5)$$

where the high-precision numbers come from the QCD evaluation in [40]. As expected, this expression is logarithmically and linearly sensitive to the cutoff  $q^*$ , canceling the opposite sensitivities in the soft sector in Eqs. (4.1) and (4.2). This corresponds to stating that the IR limit of Eq. (4.4) is

$$\mathcal{C}_{\text{hard}}^{\text{SYM}}(q_{\perp} \ll T) = \frac{g^4 C_R T m_E^2}{q_{\perp}^4} - \frac{g^4 C_R C_A T^2}{4q_{\perp}^3} + \mathcal{O}\left(\frac{g^4 T}{q_{\perp}^2}\right). \quad (4.6)$$

As noted in [19, 40], the IR linear sensitivity to the cutoff, caused by the second term above, emerges when taking the double limit  $q_{\perp} \rightarrow gT$  and  $p \rightarrow gT$  in Eq. (4.4). Because of the IR enhancement of the Bose–Einstein distribution, only bosons cause this contribution. Since in  $\mathcal{N} = 4$  SYM one has four times as many bosons to scatter from than in QCD ( $2C_A$  gluons and  $6C_A$  scalars versus just  $2C_A$  gluons), this contribution is four times larger than in QCD. The cancellation of  $q^*$ -dependent terms between Eqs. (4.1), (4.2) and (4.5) means that, at the interface of the two regions,  $gT \ll q_{\perp} \ll T$ , the soft and hard expressions for  $\mathcal{C}(q_{\perp})$  must agree. This is trivially verified for the first term in Eq. (4.6) and Eq. (3.4). For what concerns the second term in Eq. (4.6), we find that the UV limit of  $\delta\mathcal{C}(q_{\perp})$  in Eq. (3.7) is

$$\delta\mathcal{C}(q_{\perp} \gg gT) = -\frac{g^4 C_R C_A T^2}{4q_{\perp}^3} + \mathcal{O}\left(\frac{1}{q_{\perp}^5}\right), \quad (4.7)$$

which matches Eq. (4.6). It is this term that causes the negative, linear dip at the origin in Fig. 6 (recall that the dimensionally-regularized Fourier transform of  $1/q_{\perp}^3$  in 2 dimensions is  $-x_{\perp}/(2\pi)$ ).<sup>5</sup>

Summing Eqs. (4.1), (4.2) and (4.5) we obtain the NLO  $\hat{q}$  of the  $\mathcal{N} = 4$  SYM plasma, which reads

$$\hat{q} = \frac{\lambda^2 T^3}{6\pi} \left[ 6 \log\left(\frac{T}{m_E}\right) + 7 \frac{\zeta(3)}{\zeta(2)} \log\left(\frac{q_{\text{max}}}{T}\right) - 0.4212546701382088 \dots \right. \\ \left. + \frac{m_E}{T} \left( \xi_E^{(\text{NLO})} + \xi_S^{(\text{NLO})} \right) \right] + \mathcal{O}(\lambda^3), \quad (4.8)$$

where the second line contains the NLO contributions:  $\xi_E^{(\text{NLO})} = \frac{3}{16\pi}(3\pi^2 + 10 - 4 \log 2) \simeq 2.198500$  is the one also appearing in QCD, and  $\xi_S^{(\text{NLO})} = \frac{9}{4\sqrt{2}\pi}(1 - \log 2) \simeq 0.155399$  is the genuine SYM-specific contribution from soft scalars. It is thus worth noting that this genuine SYM contribution has numerically a small impact, being less than 10% of the gluon contribution shared with QCD. This should not be interpreted to mean that the overall scalar contribution is small: recall that one half of  $m_E$  and  $m_S$  is due to (hard) scalars, as shown in Eq. (3.3). In other words, taking the QCD expression for  $\delta\hat{q}$  and changing the Debye mass  $m_E$  from the QCD to the SYM value, thus including the large hard scalar contribution thereto, represents a good approximation to Eq. (4.2). As we shall show in

---

<sup>5</sup>The  $1/q_{\perp}^3$  term was also extracted in the hard sector in the electroweak theory in [54] (see Eq. (D.6) there), finding  $-g^2 C_R T^2 / (16q_{\perp}^3)(C_A + N_S T_F)$ , where  $N_S = 1$  is the complex, fundamental Higgs scalar doublet. Since  $\mathcal{N} = 4$  SYM has 6 *real*, adjoint scalars, which implies the replacement  $N_S T_F \rightarrow n_s C_A / 2 = 3C_A$ , this expression is consistent with ours in Eq. (4.7).

Sec. 5, the overall large scalar contribution to  $\delta\mathcal{C}(q_\perp)$ , in particular its limiting form in Eq. (4.7), has a significant impact on the NLO collinear splitting rate.

Let us quote the QCD results from [19, 40]

$$\hat{q}_{\text{QCD}} = \frac{g^4 C_R T^3}{6\pi} \left\{ C_A \left[ \log\left(\frac{T}{m_E}\right) + \frac{\zeta(3)}{\zeta(2)} \log\left(\frac{q_{\text{max}}}{T}\right) - 0.0688854926766592 \dots \right] \right. \\ \left. + N_f T_F \left[ \log\left(\frac{T}{m_E}\right) + \frac{3}{2} \frac{\zeta(3)}{\zeta(2)} \log\left(\frac{q_{\text{max}}}{T}\right) - 0.072856349715786 \dots \right] \right. \\ \left. + C_A \frac{m_E}{T} \xi_E^{(\text{NLO})} \right\}, \quad (4.9)$$

where in QCD  $m_E^2 = g^2 T^2 (C_A + N_f T_F)/3$  and the term on the third line is the NLO contribution. We note that in QCD the NLO correction to  $\hat{q}$  is large, as found in [19]: already at  $\alpha_s = 0.1$  it represents a 100% correction: more precisely, for  $N_f = 3$ ,  $q_{\text{max}} = 50T$  and  $\alpha_s = 0.1$  one finds  $\hat{q} \approx 1.11 C_R T^3$  in LO QCD,  $\hat{q} \approx 1.87 C_R T^3$  in NLO QCD. The very large  $q_{\text{max}} = 50T$  has been chosen to give a conservative estimate of the NLO/LO ratio, as the LO contribution grows logarithmically in  $q_{\text{max}}$ : for a smaller  $q_{\text{max}} = 10T$  one would have  $\hat{q} \approx 0.59 C_R T^3$  in LO QCD,  $\hat{q} \approx 1.35 C_R T^3$  in NLO QCD. In the SYM case we have two observations: on the one hand, at LO in the hard region there is an extra, large contribution from scalars, which is exactly three times the gluon contribution, together with a significant group-theory boost to the fermion contribution with respect to QCD, while at NLO the numerical factor multiplying the expansion parameter  $m_E/T$  changes by a small amount with respect to QCD, thus suggesting smaller relative NLO contributions. On the other hand, as we have mentioned, in  $\mathcal{N} = 4$  SYM  $m_E/T$  is larger than in QCD at a given  $g$ , due to the large scalar contribution thereto. We then obtain, for  $\alpha_s = 0.1$ ,  $N_c = 3$  and  $q_{\text{max}} = 50T$  we find in LO SYM  $\hat{q} \approx 10.20 T^3$  and in NLO SYM  $\hat{q} \approx 15.07 T^3$  (for  $q_{\text{max}} = 10T$  we have  $\hat{q} \approx 3.99 T^3$  in LO SYM,  $\hat{q} \approx 8.87 T^3$  in NLO SYM).

Before we elaborate further on the NLO/LO ratio, we must address the fact that, as pointed out in [19], Eqs. (4.8) and (4.9) suffer from truncation effects arising from the intermediate regulator  $q^*$ . In other words, Eqs. (4.8) and (4.9) have been obtained for  $m_E \ll q^* \ll T$  and can thus become ill-behaved once  $m_E \sim T$  ( $\lambda \sim 1$ ). This is particularly important at leading order (i.e. omitting the terms on the final line), where, for large enough  $m_E \sim gT$ , the entire expressions become negative. Besides, the regulator makes a plot of  $\mathcal{C}(q_\perp)$  for all  $q_\perp$  challenging. A solution to these two problems, introduced in [40] and used for the plots in [19], is to introduce a new *resummed scheme* for the LO  $\mathcal{C}(q_\perp)$ , which reads (see also [55] where a different resummation is performed<sup>6</sup>)

$$\mathcal{C}^{(\text{LO})}(q_\perp) \equiv \mathcal{C}_{\text{hard}}(q_\perp) \times \frac{q_\perp^2}{q_\perp^2 + m_E^2}. \quad (4.10)$$

At small  $m_E/T$  (small  $g$ ) it is easy to see that this expression, when plugged in Eq. (2.7), reproduces the LO result for  $\hat{q}$  plus some higher-order terms. In the IR,  $\mathcal{C}_{\text{hard}}(q_\perp \ll T)$

---

<sup>6</sup>In more detail, the authors of Ref. [55] resum HTL self-energies for exchanged momenta smaller than  $q^*$ , with  $gT \ll q^* \ll T$ , and full self-energies above that cut-off.

is dominated by the first term in Eq. (4.6) and we thus reproduce Eq. (3.4), the soft contribution to Eq. (2.8). In the hard region, the factor  $q_{\perp}^2/(q_{\perp}^2 + m_E^2)$  becomes 1, up to corrections of order  $m_E^2/q_{\perp}^2 \sim g^2$ . However, due to these partially resummed higher-order corrections, the resulting curve extrapolates better to higher values of  $g$ .

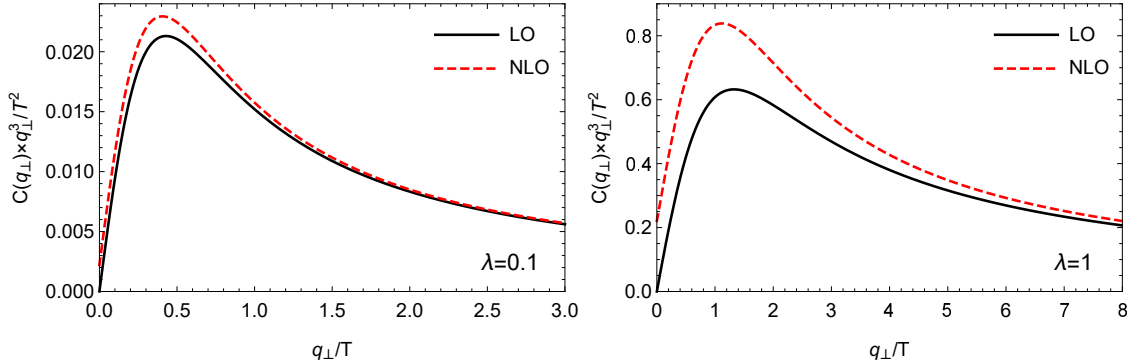


**Figure 7.**  $C(q_{\perp}) \times q_{\perp}^3/T^2$  as a function of  $q_{\perp}/T$  for different values of the coupling. The solid black lines come from Eq. (4.10), while the dashed red ones from Eq. (4.11). The area under the curves is directly proportional to  $\hat{q}$ .

At NLO one could simply add  $\delta\mathcal{C}(q_{\perp})$  to this equation, which is the approach followed in [19]. However, this double-counts some NLO contributions, as  $\mathcal{C}_{\text{hard}}(q_{\perp} \ll T)$  contains also the subleading second term in Eq. (4.6) giving rise to the linear-in- $q^*$  term in Eq. (4.5), and which is matched by the UV limit of  $\delta\mathcal{C}(q_{\perp})$ , Eq. (4.7). Hence, we propose instead the following scheme for the NLO  $C(q_{\perp})$

$$C^{(\text{NLO})}(q_{\perp}) \equiv \mathcal{C}_{\text{hard}}(q_{\perp}) + \mathcal{C}_{\text{soft}}^{(\text{LO})}(q_{\perp}) + \mathcal{C}_{\text{soft}}^{(\text{NLO})}(q_{\perp}) - \frac{2\lambda^2 T^3}{q_{\perp}^4} + \frac{\lambda^2 T^2}{4q_{\perp}^3}. \quad (4.11)$$

Contrary to the leading-order one, it is a *strict* scheme: in the IR  $\mathcal{C}_{\text{hard}}(q_{\perp})$  is approximated by the last two terms in this equation, as shown in Eq. (4.6). Hence  $\mathcal{C}_{\text{hard}}(q_{\perp})$  cancels against these two terms there (up to terms of order  $\frac{\lambda^2 T}{q_{\perp}^2}$ ), leaving just  $\mathcal{C}_{\text{soft}}^{(\text{LO})}(q_{\perp}) + \mathcal{C}_{\text{soft}}^{(\text{NLO})}(q_{\perp})$ . In the UV, conversely, the last two terms cancel the UV limits of the soft terms, leaving just  $\mathcal{C}_{\text{hard}}(q_{\perp})$ . It is easy to see that Eq. (4.11), when inserted in Eq. (2.7), reproduces Eq. (4.8),<sup>7</sup> which further confirms that our Eq. (4.8) is a strict prescription for  $\hat{q}$  at NLO. We plot our choices for  $C(q_{\perp})$  at LO and NLO in solid black and dashed red in Figs. 7 and 8 for different values of the couplings and multiplied by  $q_{\perp}^3$ , so that the area under these curves is directly proportional to  $\hat{q}$ . Similarly to the QCD plots in [19], we see how the two curves differ more and more as the coupling is increased. At  $\lambda = 10$ , which is a typical “intermediate” coupling in heavy ion phenomenology, corresponding, for  $N_c = 3$ , to  $\alpha_s \approx 0.26$ , the NLO corrections have completely overtaken the LO curve, signaling a convergence problem of the perturbative expansion for this observable.

In Fig. 9 we plot instead the NLO/LO ratio for  $\hat{q}$  in SYM and  $N_c = N_f = 3$  QCD. At NLO we use the strict expression in Eqs. (4.8) and (4.9). At LO, the “strict” curves

<sup>7</sup>Up to discrepancies of order  $1/q_{\text{max}}$  from truncating the integration at  $q_{\text{max}}$ , whereas the finite terms  $\xi^{(\text{NLO})}$  in Eq. (4.8) have been obtained with  $q_{\text{max}} \rightarrow \infty$ .

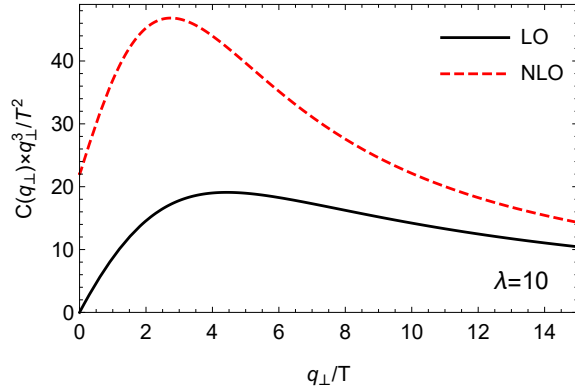


Figure 8.  $C(q_\perp) \times q_\perp^3 / T^2$  as in Fig. 7, at larger coupling.

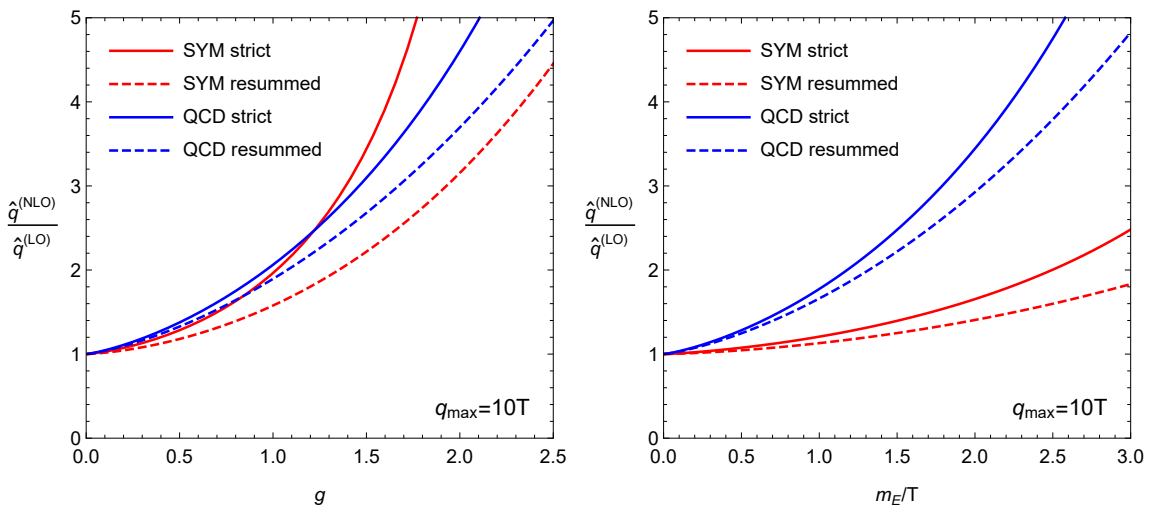


Figure 9. The NLO/LO ratios for  $\hat{q}$  in SYM and QCD. For the latter theory  $N_c = N_f = 3$ , for the former  $N_c = 3$  on the left, while the r.h.s. is  $N_c$ -independent.  $q_{\max} = 10T$  in both plots. We refer to the text for the precise references to the equations being plotted.

use again those expressions omitting the NLO terms in their final lines. The “resummed” curves are instead obtained by numerical integration of Eq. (4.10), with Eqs. (4.3) and (4.4) for QCD and SYM respectively. The plot on the l.h.s. is as a function of  $g$  (with  $N_c = 3$  for SYM as well) and shows that NLO corrections are large in both theories at equal values of the coupling. Furthermore, the size of the NLO corrections is *similar* in the two theories and the discrepancy between the two schemes provides a first estimate of the truncation uncertainty. On the right we plot the same equations as a function of  $m_E$ : as expected, NLO corrections are significantly smaller in SYM at equal Debye mass.

Finally, we observe that Eq. (4.11) could also have applications in QCD where, to the best of our knowledge, it has not appeared in the literature. In particular, we find that it is much better suited than Eq. (4.10) to a numerical Fourier transform. Eq. (4.10) requires to sample two numerical parameters,  $m_E/T$  (or  $g$ ) and  $x_\perp T$ , while the Fourier transforms



of the individual terms in Eq. (4.11) depend either on  $x_\perp m_E$  or on  $x_\perp T$ , and many of them can be obtained analytically. We have tested that the numerical Fourier transform of  $\mathcal{C}_{\text{hard}}(q_\perp)$  is not particularly complicated once a fine enough sampling of  $\mathcal{C}_{\text{hard}}(q_\perp)$  has been obtained. This procedure leads to an expression for  $\mathcal{C}'(x_\perp)$  at NLO that interpolates smoothly from  $x_\perp T \sim 1$  to  $x_\perp m_E \sim 1$  and would thus be helpful for solutions of the collinear splitting equations in cases where the energy of the mother parton is much larger than the temperature, requiring to account for transverse kicks at the scale  $T$  beyond those at the scale  $m_E$  normally included in the AMY formalism [63, 64].

#### 4.1 Comparisons with AdS/CFT results

Refs. [33–35] computed the Wilson loop in Eq. (2.2) for an adjoint source at strong coupling through the AdS/CFT correspondence. In its validity region, the result is Gaussian in  $x_\perp$ , i.e.

$$\langle W(x_\perp, L) \rangle_{\text{AdS}} \approx \exp\left(-\frac{\pi^{3/2}\Gamma(3/4)}{4\Gamma(5/4)}\sqrt{\lambda}T^3 x_\perp^2 L\right). \quad (4.12)$$

From our discussion in Sec. 2 it follows that  $\langle W(x_\perp, L) \rangle = \exp(-\hat{q}x_\perp^2 L/4)$  at small  $x_\perp$  and thus [33–35]

$$\hat{q}_{\text{AdS}} = \frac{\pi^{3/2}\Gamma(3/4)}{\Gamma(5/4)}\sqrt{\lambda}T^3. \quad (4.13)$$

This result does not require a UV regulator: intuitively, the probability distribution  $P(q_\perp)$ , which, as remarked in Footnote 3, is the Fourier transform of  $\langle W(x_\perp, L) \rangle$  and which is related, but not equal, to  $\mathcal{C}(q_\perp)$  [35, 43, 55], is also a Gaussian, with a finite second moment,  $\hat{q}$ . In other words, a conformal, strongly coupled description stays strongly coupled at all scales, while the need for a regulator at weak coupling arises from the  $1/q_\perp^4$  UV tail of the  $2 \leftrightarrow 2$  scatterings, i.e. rare large angle scatterings, oftentimes termed *Molière scatterings* [65, 66]. But such a quasi-particle picture cannot ever emerge in a strongly-coupled CFT, in contrast with asymptotically-free QCD.

Furthermore, Eqs. (4.12) and (4.13), although obtained for  $\lambda \rightarrow \infty$ , depend on  $\lambda$ . This, together with the  $q_{\text{max}}$  dependence of the weak-coupling result, make an attempt to extrapolate the weak- and strong-coupling results toward each other ill-posed for  $\hat{q}$ . Observable quantities like the thermal photon rate or the shear viscosity, which are  $\lambda$ -independent at strong coupling and regulator-independent at weak coupling, would make for much more sensible candidates for this type of comparison: our work in determining  $\hat{q}$  and  $\mathcal{C}(q_\perp)$  at NLO represents an important stepping stone towards NLO evaluation of these quantities.

However, there is still an important comparison that we can make and draw lessons from. Motivated by the  $\sqrt{\lambda}$  scaling in Eq. (4.13), Ref [34] conjectured that, at strong coupling,  $\hat{q}$  should scale like the square root of the entropy density  $s$ , i.e.

$$\frac{\hat{q}_{\text{QCD}}}{\hat{q}_{\text{SYM}}} \sim \sqrt{\frac{s_{\text{QCD}}}{s_{\text{SYM}}}} = \sqrt{\frac{47.5}{120}} \approx 0.63, \quad (4.14)$$

where the entropy densities have been taken in the non-interacting limit for  $N_c = 3$  and  $N_f = 3$ . The ratio does not change qualitatively at stronger couplings, where the SYM

entropy becomes (at large  $N_c$ , though) 3/4 of the value above [67], as do to a good degree lattice QCD results in the transition region (see e.g. [68, 69]) as well.

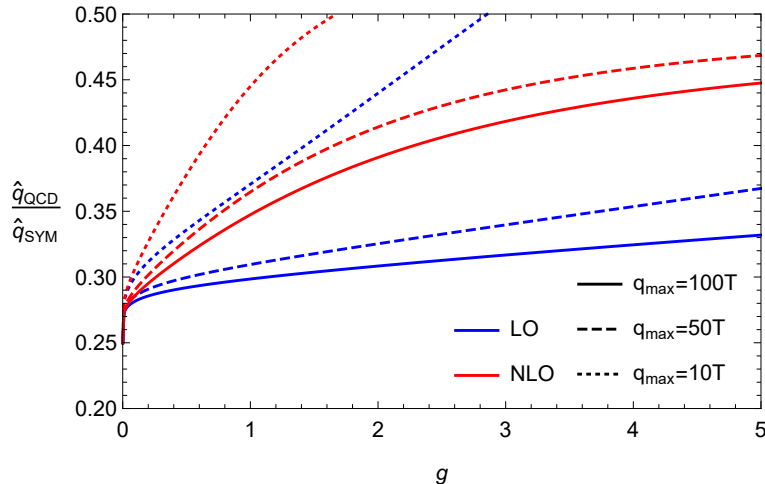


**Figure 10.** The ratio of  $\hat{q}$  for an adjoint QCD source to that in  $\mathcal{N} = 4$  SYM for three different values of  $q_{\text{max}}$  as a function of the coupling  $g$ , at LO (blue) and NLO (red). The NLO SYM curves come from Eq. (4.8) and the QCD ones from (4.9). At LO we instead integrate numerically Eq. (4.10) in the two theories up to  $q_{\text{max}}$ . In both cases we have fixed  $N_c = 3$ , in the case of QCD  $N_f = 3$ . We truncate the curves for the smaller values of  $q_{\text{max}}$  shortly before the LO strict prescription would start to break down, which we take as an indicator of the point where the perturbative results are becoming unreliable, as the scale separation between  $q_{\text{max}}$ ,  $T$  and  $m_E$  is disappearing (see also Fig. 9).

At weak coupling, we are now in the position of examining the QCD/SYM ratio at leading- and next-to-leading order, as we do in Fig. 10 as a function of the coupling for three different values of  $q_{\text{max}}$ . At NLO we choose our strict prescription, Eqs. (4.8) and (4.9), while for LO we choose the resummed prescription in Eq. (4.10). In the QCD case we consider the  $R = A$ , i.e. take the  $\hat{q}$  relevant for gluons. As the plot shows, the curves start from 0.25, which is the zero-coupling limit for this ratio for  $N_c = 3$  and  $N_f = 3$ , and then grow to be in the ballpark of 0.4, which does not differ too much from Eq. (4.14), even though, as an inspection of Eqs. (4.8) and (4.9) shows, the dependence on the number and type of degrees of freedom is not in the form of that of the square root of the entropy density. We recall that the  $\hat{q}$  relevant for quarks is obtained through an extra factor of  $C_F/C_A = 4/9$ . (Casimir scaling holds to NLO, as Eq. (4.9) shows.)

In summary, if  $q_{\text{max}}$  in QCD is chosen at a value of a few times/10 times the temperature, so as to encompass all the region that can be considered strongly coupled, leaving the UV Molière tail to perturbation theory, then a recipe for using the AdS/CFT results for  $\hat{q}$  with a rescaling factor of order 1/2 would not be inconsistent with our results for the QCD/SYM ratio at weak coupling. We also point out that in the region  $q_{\perp} \lesssim E$ , which is excluded from our approach, as argued in Sec. 2, the transferred momentum affects the kinematics of the hard parton and the eikonal, Wilson-line based approach fails. We refer

to [70] for calculations of Molière scattering without the eikonal approximation.

## 5 Collinear radiation rate

As we mentioned previously,  $\mathcal{C}(q_\perp)$  and  $\hat{q}$  are important ingredients in the determination of the medium-induced, collinear radiation rate. At weak coupling, the leading-order photon and gluon radiation rates have been determined in [63, 71] in QCD and extended to  $\mathcal{N} = 4$  SYM in [9, 15]. In QCD they have been extended to NLO in [21, 42]. As a first application of our results of Sec. 3, we now set out to extend the  $\mathcal{N} = 4$  SYM photon rate to NLO. The extension to the gluon radiation rate is also straightforward, as it requires the adaptation of the methodology used to extend the LO gluon radiation rate to NLO to the extra scalar  $\rightarrow$  scalar, gluon process of  $\mathcal{N} = 4$  SYM.

The thermal photon production rate<sup>8</sup> at leading order is given by [9]

$$(2\pi)^3 \frac{d\Gamma_\gamma}{d^3k} = \frac{1}{2k} g^{\mu\nu} W_{\mu\nu}^<(K), \quad (5.1)$$

where  $k$  is the photon's momentum and  $W_{\mu\nu}^<(K)$  is the backward Wightman two-point function of the  $U(1)$  current

$$W_{\mu\nu}^<(K) = \int d^4X e^{-iK \cdot X} \langle J_\mu(0) J_\nu(X) \rangle. \quad (5.2)$$

This rate receives LO contributions from Compton-like  $2 \leftrightarrow 2$  scatterings and from collinear radiation, that is, collinear bremsstrahlung induced by the soft scatterings, governed by  $\mathcal{C}(q_\perp)$ , from the charged, hard ( $p \sim T$ ) Weyl fermions and scalars, and its crossed process, collinear pair annihilation of the charged particles into the photon. Collinearity ensues from the small momentum transfer from soft scatterings, which in turn causes an enhancement to these rates, which would naively seem suppressed with respect to the  $2 \leftrightarrow 2$  component. Furthermore, collinear emissions imply long formation times, which turn out to be of the same order of the inverse rate given by  $\mathcal{C}(q_\perp)$ , causing Landau-Pomeranchuk-Migdal (LPM) interference and requiring resummation.

The LO collinear photon production rate, accounting for LPM resummation, is given by [9]

$$\begin{aligned} \gamma(k) &\equiv \frac{4\pi}{(N_c^2 - 1)g^2 N_c T^2 n_f(k)} g^{\mu\nu} W_{\mu\nu}^<(K) \Big|_{\text{coll}} \\ &= \int_{-\infty}^{\infty} dp^+ \left[ \frac{n_F(k+p^+)(1 - n_F(p^+))(p^{+2} + (k+p^+)^2)}{4n_F(k)p^{+2}(p^+ + k)^2} + \frac{n_B(k+p^+)(1 + n_B(p^+))}{2n_F(k)p^+(k+p^+)} \right] \\ &\times \frac{1}{g^2 N_c T^2} \int \frac{d^2 p_\perp}{(2\pi)^2} \text{Re}[2\mathbf{p}_\perp \cdot \mathbf{f}(\mathbf{p}_\perp, p^+, k)], \end{aligned} \quad (5.3)$$

where the normalization of  $\gamma(k)$  has been chosen as the leading-log coefficient of the  $2 \leftrightarrow 2$  component, which we do not consider here. The photon momentum  $k$  has been chosen

<sup>8</sup>  $\mathcal{N} = 4$  SYM does not contain a photon. Ref. [9] gauged a  $U(1)$  subgroup of the  $R$ -current to mimic electromagnetic interactions in SYM. Two Weyl fermions and two scalars become charged under this  $U(1)$  interaction.

along the  $z$  direction. The  $n_F$ - and  $n_B$ -proportional terms are the contribution from bremsstrahlung from (pair annihilation of) fermions and scalars respectively. The function  $\mathbf{f}(\mathbf{p}_\perp, p^+, k)$  is the solution of the following integral equation which resums an infinite number of soft scatterings, thus accounting for LPM interference

$$2\mathbf{p}_\perp = \frac{ik(p_\perp^2 + m_\infty^2)}{2p^+(k + p^+)} \mathbf{f}(\mathbf{p}_\perp, p^+, k) + \int \frac{d^2q_\perp}{(2\pi)^2} \mathcal{C}(q_\perp) [\mathbf{f}(\mathbf{p}_\perp, p^+, k) - \mathbf{f}(\mathbf{p}_\perp + \mathbf{q}_\perp, p^+, k)]. \quad (5.4)$$

The first term on the r.h.s. is a kinetic term: it encodes the energy difference between the final and initial states, caused by the soft scatterings described by second term, the collision operator.  $m_\infty$  in the kinetic term is the thermal asymptotic mass of the emitter fermions and scalars, which for  $p \sim T$  obey the dispersion relation  $p_0 = \pm \sqrt{p^2 + m_\infty^2}$ . In  $\mathcal{N} = 4$  SYM these asymptotic masses preserve supersymmetry, as they are the same for all species (gluons, fermions and scalars):  $m_\infty^2 = m_E^2/2 = m_S^2 = \lambda T^2$  at leading order [62].

NLO  $\mathcal{O}(g)$  corrections to Eq. (5.3) can enter only in the two inputs that are sensitive to the  $gT$  scale, as proven in [21]. These are  $\mathcal{C}(q_\perp)$ , which we have just computed to NLO, and  $m_\infty$ , whose  $\mathcal{O}(g)$  correction has been computed in [62], finding  $\delta m_\infty^2 = -g^3 C_A^{3/2} T^2 (3 + \sqrt{2}) / (2\pi)$ . Hence, to find the NLO corrections to  $\gamma(k)$ ,  $\mathbf{f}$  can be treated as an expansion in powers of  $\delta m_\infty^2$  and  $\delta \mathcal{C}$ . The zeroth-order reproduces the LO expression, and the first order in each of the two corrections gives  $\gamma^{\delta m}$  and  $\gamma^{\delta \mathcal{C}}$ , so that  $\gamma^{(\text{NLO})} = \gamma^{(\text{LO})} + \gamma^{\delta m} + \gamma^{\delta \mathcal{C}}$ . In order to determine numerically these functions, it is convenient to Fourier-transform Eq. (5.4) in  $x_\perp$ -space, where it becomes a two-dimensional Schrödinger-like equation with an imaginary potential given by  $\mathcal{C}'(x_\perp)$  [72]. We refer to [21] for details on the strategy to solve Eq. (5.4) at NLO.

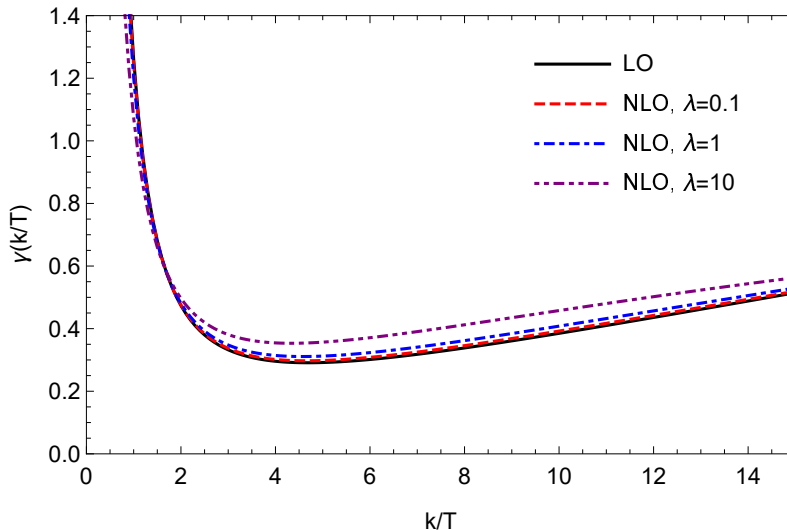


**Figure 11.** The collinear photon rate in  $\mathcal{N} = 4$  SYM. We plot the LO results [9] in solid black and the NLO results at different couplings in various colors and dashing patterns.

In Fig. 11 we plot our NLO results for  $\gamma$ . As the figure clearly show, the NLO corrections turn out to be small: even at  $\lambda = 10$  they represent at most a 30% decrease in the

IR and a 20% increase at  $k \approx 5T$ . This is in sharp contrast with the results in NLO QCD [21], where for  $\alpha_s = 0.3$  the correction is approximately a 100% increase.

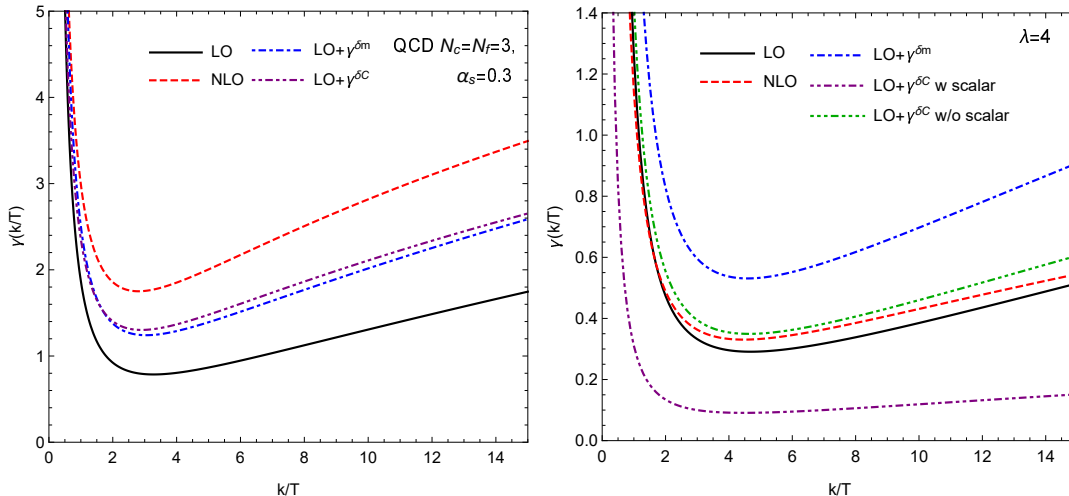


**Figure 12.** Left: the separate sum of the LO  $\gamma$  with each of the two NLO corrections  $\gamma^{\delta m}$  and  $\gamma^{\delta \mathcal{C}}$  in QCD with  $N_c = N_f = 3$ ,  $\alpha_s = 0.3$ . The results are taken from [21] and are normalized by the QCD leading-log coefficient. On the right we plot the same in  $\mathcal{N} = 4$  SYM for  $\lambda = 4$ , with the addition of the extra curve for  $\gamma^{\delta \mathcal{C}}$  where  $\delta \mathcal{C}$  is taken without the scalar contribution (3.6), corresponding to the QCD  $\delta \mathcal{C}$ . In both cases the full NLO collinear emission rate,  $\gamma^{(\text{NLO})}$ , is a sum of the two corrections  $\gamma^{\delta m}$  and  $\gamma^{\delta \mathcal{C}}$  and of the leading order result  $\gamma^{(\text{LO})}$ .

To investigate this large discrepancy, let us look at Fig. 12. On the left we plot the QCD results of [21] (with  $N_c = N_f = 3$ , normalized by the QCD leading-log coefficient), split in the contribution of  $\delta m_\infty^2$  and  $\delta \mathcal{C}$  for  $\alpha_s = 0.3$ . On the right we plot the same for SYM. We see that the  $\gamma^{\delta m}$  curves have a very similar behavior, but the  $\gamma^{\delta \mathcal{C}}$  do not. In fact, the latter is positive and comparable with  $\gamma^{\delta m}$  in QCD, while it is negative in SYM. These facts can be understood as follows: the  $\gamma^{\delta m}$  correction is proportional to  $\delta m_\infty^2/m_\infty^2$ . In QCD this is  $-2m_E/(\pi T)$ , which, for  $N_c = N_f = 3$ , is approximately  $-0.78g$ . In SYM it approximates  $-0.70\sqrt{\lambda}$ , so for our choice of  $\lambda = 4$  and  $\alpha_s = 0.3$ , for which  $g \approx \sqrt{\lambda} = 2$ , we expect the observed similar behavior. For the  $\delta \mathcal{C}$  correction, on the other hand, there are two major factors to account for. As the SYM plot shows, if we omit the scalar contribution, Eq. (3.6), from  $\delta \mathcal{C}$ , corresponding to using the  $\delta \mathcal{C}$  of QCD, the resulting correction becomes positive, as in QCD. And as the discussion in Secs. 3 and 4, together with Fig. 6, illustrated, the scalar contribution has the effect of making  $\delta \mathcal{C}'(x_\perp)$  smaller, accentuating its negative dip at small  $x_\perp$ , due to the large UV,  $\lambda^2/q_\perp^3$ -proportional term which is three times the one in the gluon contribution. Simple positivity argument imply that it is the negative part of  $\delta \mathcal{C}'(x_\perp)$  that causes the observed negative  $\gamma^{\delta \mathcal{C}}$ . Furthermore,  $\gamma^{\delta \mathcal{C}}$  is proportional to  $g^2 C_{AT}/m_E$ , which is the ratio of the coefficients of  $\delta \mathcal{C}'(x_\perp)$  and  $\mathcal{C}'(x_\perp)$ . In  $N_c = N_f = 3$  QCD this approximates to  $2.45g$ , while in SYM it is the much smaller  $0.71\sqrt{\lambda}$ , which goes to explain why the curve without the scalar contribution to  $\mathcal{C}$ , that is with the QCD  $\delta \mathcal{C}$ , has a much smaller impact than in QCD.

## 6 Summary and conclusions

In this paper we have investigated the transverse scattering kernel  $\mathcal{C}(q_\perp)$  and the transverse momentum broadening coefficient  $\hat{q}$  at NLO in perturbative  $\mathcal{N} = 4$  SYM, including thus  $\mathcal{O}(g)$  effects from soft bosons. The NLO correction to the former,  $\delta\mathcal{C}(q_\perp)$ , has been evaluated in Sec. 3 using the analytical mapping to a dimensionally-reduced Euclidean theory introduced in [19]. Our analysis in that section identified all diagrams with contributions from the scalar fields of  $\mathcal{N} = 4$  SYM, that are absent in the QCD calculation [19] and that we evaluated, yielding our result for the NLO correction to  $\mathcal{C}$ , Eq. (3.7). We also obtained the Fourier-transformed, impact-parameter space expression in Eq. (3.10), which is more useful in the solution of the collinear rate equation and which shows how the NLO correction is negative at small  $x_\perp$  and how the scalar contribution boosts this feature, as shown in Figs. 5 and 6.

In Sec. 4 we used the NLO expression for the scattering kernel to determine  $\hat{q}$  at NLO, which may be found in Eq. (4.8). This required also obtaining the contribution from the scale  $T$  to  $\hat{q}$  and understanding how the soft and hard contributions match in the interface region between the two scales. In particular, we found that the hard contribution from the SYM scalars is three times that from gluons, also present in QCD. The NLO contribution is proportional to the Debye mass  $m_E$ , which is also boosted by a large hard scalar contribution in a threefold ratio with the gluon one. However, the soft scalar loops we computed give a numerically small contribution, of the order of 10% of the soft gauge loops already computed in QCD.

We then used our NLO results to try to understand how to best bridge between QCD and SYM. The strong-coupling AdS/CFT calculations [33–35] are not directly comparable, because of the distinctive UV-divergences that arise at weak coupling in  $\hat{q}$  from large-angle scatterings. However, if one considers  $\hat{q}$  as an effective parameter describing scatterings with the medium up to some  $q_{\max}$  below which a strong-coupling description is considered applicable, then a prescription for extrapolating the AdS/CFT results to the different degrees of freedom of QCD is necessary. Ref. [34] conjectured that a rescaling by the square root of the ratio of the entropy densities in the two theories would provide a good measure. We have examined the QCD/SYM ratio for  $\hat{q}$  at weak coupling at NLO, see Fig. 10, and found that it ranges from being half of the conjectured ratio at small couplings to 2/3 of it once intermediate couplings are approached, thus potentially indicative of an extrapolation to the conjectured strong-coupling ratio. Furthermore, our weak-coupling ratio was not widely different between leading- and next-to-leading order. In other words, the NLO/LO ratio is similar in QCD and SYM for  $\hat{q}$  at fixed coupling, as shown explicitly by our Fig. 9.

Our examination of the collinear splitting rate in Sec. 5 may however suggest that no universal lessons can be drawn from these particular NLO corrections. Indeed, we found that the NLO collinear splitting rate is a small ( $\mathcal{O}(10 - 20\%)$ ) modification of LO in SYM even at  $\lambda = 10$ , see Fig. 11, in sharp contrast to QCD where it is essentially twice the LO rate for  $\alpha_s = 0.3$ . The reason is that these corrections are very sensitive to the precise nature of the theory and its degrees of freedom. In QCD both the  $\mathcal{O}(g)$  shift in the dispersion relation and the  $\mathcal{O}(g)$  shift in  $\mathcal{C}(q_\perp)$  result in positive corrections to the collinear

rate. The weights of these corrections are different and depend in a non-trivial way on the statistics and group theory properties of the d.o.f.s: for  $N_c = N_f = 3$  QCD the corrections are almost identical (see Fig. 12). In SYM, on the other hand, these weights are in a very different ratio and furthermore the correction due to  $\delta\mathcal{C}(q_\perp)$  is negative, for reasons we can attribute to the large scalar contribution to  $\mathcal{C}(q_\perp)$  at the interface between the soft and hard regions. Hence the two contributions experience a large cancellation, which is reminiscent of the large, accidental cancellations found between different NLO contributions in the QCD photon rate [21], which was observed to be dependent on the specifics of the d.o.f.s. We thus conclude that the cancellation we observe is also largely accidental and not motivated by any particular symmetry such as supersymmetry: QCD with scalar quarks in place of fermion ones would also be susceptible to such a cancellation, its precise amount sensitive to how many scalar quarks are introduced and the representation they transform under.

Indeed, it would be interesting to see how the SYM photon rate is modified at NLO. Besides these collinear corrections we have computed, one would need the scalar contribution to the other kinematical regions identified in the QCD calculation, i.e. the semi-collinear and soft ones. While the former seems rather straightforward, a preliminary analysis of the latter shows that it would require a non-trivial calculation using the light-cone sum-rules of [21, 42]. Similar work would be required also for an NLO computation of the shear viscosity and other transport coefficients. It would be very interesting to understand whether the large corrections found in [22] for QCD – and almost entirely driven by its large  $\delta\hat{q}$  – also appear in the SYM case, with the comparable  $\delta\hat{q}$  we have found. Indeed, a major unanswered point raised by [22] is the identification of the physics responsible for these large corrections and the subsequent reorganization of the perturbative series.

To this end, one of the possible pathways is the lattice determination of the  $gT$ -scale physics. The mapping to the Euclidean theory we have exploited for our computation in Sec. 3 allows also for lattice-EQCD determinations of  $\mathcal{C}(q_\perp)$  and related observables whose soft contribution is dominated by the Matsubara zero mode. Indeed, a first study of  $\hat{q}$  and  $\mathcal{C}'(x_\perp)$  in lattice EQCD has been carried out [58] and could be extended to ESYM without encountering any of the major issues that affect lattice discretizations of  $\mathcal{N} = 4$  SYM (see [73, 74] for reviews), as supersymmetry is broken in ESYM and fermions are absent. The conformal nature of  $\mathcal{N} = 4$  SYM may further simplify the matching to ESYM, potentially making (E)SYM a good testbed of these lattice techniques in a program, featuring our results, of more precise measurements and investigations of other observables.

## Acknowledgments

The authors would like to thank Urs Wiedemann and Krishna Rajagopal for useful conversations. This work was supported by the Korean Research Foundation (KRF) through the CERN-Korea graduate student program and was partially supported by the Graduate School of YONSEI University Research Scholarship Grants in 2017.

## A Feynman Rules of ESYM

The Feynman rules are obtained from the ESYM Lagrangian, Eq. (3.1), in a rather straightforward way. We collect them here in Feynman gauge, together with our graphical notation. The propagators read

$$i; a \text{ --- } \frac{\delta^{ab} \delta_{ij}}{p^2} \text{ --- } j; b = \frac{\delta^{ab} \delta_{ij}}{p^2} \quad : \text{ gauge}, \quad (\text{A.1})$$

$$0; a \text{ --- } \frac{\delta^{ab}}{p^2 + m_E^2} \text{ --- } 0; b = \frac{\delta^{ab}}{p^2 + m_E^2} \quad : \text{ electrostatic}, \quad (\text{A.2})$$

$$I; a \text{ --- } \frac{\delta^{ab} \delta_{IJ}}{p^2 + m_S^2} \text{ --- } J; b = \frac{\delta^{ab} \delta_{IJ}}{p^2 + m_S^2} \quad : \text{ scalar}, \quad (\text{A.3})$$

$$a \text{ --- } \frac{\delta^{ab}}{p^2} \text{ --- } b = \frac{\delta^{ab}}{p^2} \quad : \text{ ghost}. \quad (\text{A.4})$$

The three-point vertices are

$$i; a \text{ --- } \frac{\delta^{ab} \delta_{ij}}{p^2} \text{ --- } q \text{ --- } \frac{\delta^{ab} \delta_{ij}}{p^2} \text{ --- } j; b \text{ --- } \frac{\delta^{ab} \delta_{ij}}{p^2} \text{ --- } r \text{ --- } k; c = ig_E f^{abc} (\delta_{ij} (p - q)_k + \delta_{jk} (q - r)_i + \delta_{ki} (r - p)_j), \quad (\text{A.5})$$

$$i; a \text{ --- } \frac{\delta^{ab} \delta_{ij}}{p^2} \text{ --- } 0; c \text{ --- } \frac{\delta^{ab} \delta_{ij}}{p^2} \text{ --- } 0; b = ig_E f^{abc} (q - r)_i, \quad (\text{A.6})$$

$$i; a \text{ --- } \frac{\delta^{ab} \delta_{ij}}{p^2} \text{ --- } J; c \text{ --- } \frac{\delta^{ab} \delta_{ij}}{p^2} \text{ --- } I; b = ig_E \delta_{IJ} f^{abc} (q - r)_i, \quad (\text{A.7})$$

$$i; a \text{ --- } \frac{\delta^{ab} \delta_{ij}}{p^2} \text{ --- } c \text{ --- } \frac{\delta^{ab} \delta_{ij}}{p^2} \text{ --- } b = -ig_E f^{abc} r_i. \quad (\text{A.8})$$

Finally, the four-point vertices read

$$i; a \text{ --- } \frac{\delta^{ab} \delta_{ij}}{p^2} \text{ --- } j; b \text{ --- } \frac{\delta^{ab} \delta_{ij}}{p^2} \text{ --- } k; c \text{ --- } \frac{\delta^{ab} \delta_{ij}}{p^2} \text{ --- } l; d = -g_E^2 [f^{abc} f^{cde} (\delta_{ik} \delta_{jl} - \delta_{il} \delta_{jk}) + f^{ace} f^{bde} (\delta_{ij} \delta_{kl} - \delta_{il} \delta_{jk}) + f^{adc} f^{bce} (\delta_{ij} \delta_{kl} - \delta_{ik} \delta_{jl})], \quad (\text{A.9})$$

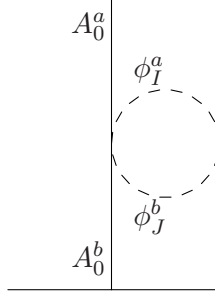
$$i; a \text{ --- } \frac{\delta^{ab} \delta_{ij}}{p^2} \text{ --- } j; b \text{ --- } \frac{\delta^{ab} \delta_{ij}}{p^2} \text{ --- } 0; c \text{ --- } \frac{\delta^{ab} \delta_{ij}}{p^2} \text{ --- } 0; d = -g_E^2 \delta_{ij} (f^{ace} f^{bde} + f^{bce} f^{ade}), \quad (\text{A.10})$$

$$i; a \text{ --- } \frac{\delta^{ab} \delta_{ij}}{p^2} \text{ --- } j; b \text{ --- } \frac{\delta^{ab} \delta_{ij}}{p^2} \text{ --- } I; c \text{ --- } \frac{\delta^{ab} \delta_{ij}}{p^2} \text{ --- } J; d = -g_E^2 \delta_{IJ} (f^{ace} f^{bde} + f^{bce} f^{ade}). \quad (\text{A.11})$$

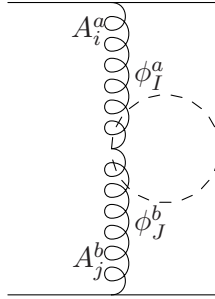


## B Scalar contributions to the one-loop diagrams in Fig. 3

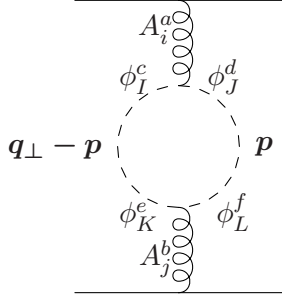
The loop contribution from the SYM scalars to  $\delta\mathcal{C}(q_\perp)$  comes from the three diagrams identified in Sec. 3. We now present the details of their explicit evaluation. The expressions below give the contribution to the self-energies  $\Pi^{00}$  and  $\Pi^{zz}$ .



$$\begin{aligned}
 &= \frac{1}{2} \left[ -g_E^2 \delta_{IJ} (f^{ace} f^{bde} + f^{bce} f^{ade}) \right] \left[ \int_p \frac{\delta^{cd} \delta_{IJ}}{p^2 + m_S^2} \right] \\
 &= -6g_E^2 C_A \delta^{ab} \int_p \frac{1}{p^2 + m_S^2},
 \end{aligned} \tag{B.1}$$



$$\begin{aligned}
 &= \frac{1}{2} \left[ -g_E^2 \delta_{zz} \delta_{IJ} (f^{ace} f^{bde} + f^{bce} f^{ade}) \right] \left[ \int_p \frac{\delta^{cd} \delta_{IJ}}{p^2 + m_S^2} \right] \\
 &= -6g_E^2 C_A \delta^{ab} \int_p \frac{1}{p^2 + m_S^2},
 \end{aligned} \tag{B.2}$$



$$\begin{aligned}
 &= \frac{1}{2} \int_p \left[ ig_E \delta_{IJ} f^{acd} (2p - q_\perp)_z \right] \left[ \frac{\delta^{df} \delta_{JL}}{p^2 + m_S^2} \right] \\
 &\times \left[ ig_E \delta_{KL} f^{bef} (q_\perp - 2p)_z \right] \left[ \frac{\delta^{ce} \delta_{KI}}{(q_\perp - p)^2 + m_S^2} \right] \\
 &= 6g_E^2 C_A \delta^{ab} \int_p \frac{2p_z^2}{(p^2 + m_S^2)((q_\perp - p)^2 + m_S^2)},
 \end{aligned} \tag{B.3}$$

where in dimensional regularization  $\int_p \equiv \int d^d p / (2\pi)^d$ , with  $d \rightarrow 3$ , and

$$\int_p \frac{1}{p^2 + m^2} = -\frac{m}{4\pi}, \tag{B.4}$$

$$\int_p \frac{p_z^2}{(p^2 + m^2)((p - q_\perp)^2 + m^2)} = -\frac{(4m^2 + q_\perp^2) \tan^{-1}(q_\perp/2m) + 2mq_\perp}{32\pi q_\perp}. \tag{B.5}$$

Upon inserting the expressions above in the propagators  $G_{00}^2$  and  $G_{zz}^2$ , the contribution of the SYM scalar fields to NLO collision kernel sums up to Eq. (3.6).

## References

- [1] J. M. Maldacena, *The Large N limit of superconformal field theories and supergravity*, *Adv.Theor.Math.Phys.* **2** (1998) 231 [[hep-th/9711200](#)].
- [2] E. Witten, *Anti-de Sitter space and holography*, *Adv.Theor.Math.Phys.* **2** (1998) 253 [[hep-th/9802150](#)].

- [3] S. Gubser, I. R. Klebanov and A. M. Polyakov, *Gauge theory correlators from noncritical string theory*, *Phys.Lett.* **B428** (1998) 105 [[hep-th/9802109](#)].
- [4] J. Casalderrey-Solana, H. Liu, D. Mateos, K. Rajagopal and U. A. Wiedemann, *Gauge/String Duality, Hot QCD and Heavy Ion Collisions*, *Cambridge University Press* (2011) [[1101.0618](#)].
- [5] G. Policastro, D. T. Son and A. O. Starinets, *The Shear viscosity of strongly coupled  $N=4$  supersymmetric Yang-Mills plasma*, *Phys. Rev. Lett.* **87** (2001) 081601 [[hep-th/0104066](#)].
- [6] P. Kovtun, D. T. Son and A. O. Starinets, *Holography and hydrodynamics: Diffusion on stretched horizons*, *JHEP* **10** (2003) 064 [[hep-th/0309213](#)].
- [7] P. Kovtun, D. T. Son and A. O. Starinets, *Viscosity in strongly interacting quantum field theories from black hole physics*, *Phys. Rev. Lett.* **94** (2005) 111601 [[hep-th/0405231](#)].
- [8] H. B. Meyer, *Transport Properties of the Quark-Gluon Plasma: A Lattice QCD Perspective*, *Eur. Phys. J.* **A47** (2011) 86 [[1104.3708](#)].
- [9] S. Caron-Huot, P. Kovtun, G. D. Moore, A. Starinets and L. G. Yaffe, *Photon and dilepton production in supersymmetric Yang-Mills plasma*, *JHEP* **0612** (2006) 015 [[hep-th/0607237](#)].
- [10] B. Hassanain and M. Schvellinger, *Plasma photoemission from string theory*, *JHEP* **1212** (2012) 095 [[1209.0427](#)].
- [11] A. Buchel, J. T. Liu and A. O. Starinets, *Coupling constant dependence of the shear viscosity in  $N=4$  supersymmetric Yang-Mills theory*, *Nucl. Phys.* **B707** (2005) 56 [[hep-th/0406264](#)].
- [12] P. Benincasa and A. Buchel, *Transport properties of  $N=4$  supersymmetric Yang-Mills theory at finite coupling*, *JHEP* **01** (2006) 103 [[hep-th/0510041](#)].
- [13] A. Buchel, *Shear viscosity of boost invariant plasma at finite coupling*, *Nucl. Phys.* **B802** (2008) 281 [[0801.4421](#)].
- [14] A. Buchel, *Shear viscosity of CFT plasma at finite coupling*, *Phys. Lett.* **B665** (2008) 298 [[0804.3161](#)].
- [15] S. Caron-Huot, S. Jeon and G. D. Moore, *Shear viscosity in weakly coupled  $N = 4$  super Yang-Mills theory compared to QCD*, *Phys. Rev. Lett.* **98** (2007) 172303 [[hep-ph/0608062](#)].
- [16] P. B. Arnold, G. D. Moore and L. G. Yaffe, *Photon emission from quark gluon plasma: Complete leading order results*, *JHEP* **0112** (2001) 009 [[hep-ph/0111107](#)].
- [17] P. B. Arnold, G. D. Moore and L. G. Yaffe, *Transport coefficients in high temperature gauge theories. 1. Leading log results*, *JHEP* **0011** (2000) 001 [[hep-ph/0010177](#)].
- [18] P. B. Arnold, G. D. Moore and L. G. Yaffe, *Transport coefficients in high temperature gauge theories. 2. Beyond leading log*, *JHEP* **0305** (2003) 051 [[hep-ph/0302165](#)].
- [19] S. Caron-Huot,  *$O(g)$  plasma effects in jet quenching*, *Phys.Rev.* **D79** (2009) 065039 [[0811.1603](#)].
- [20] J. Ghiglieri and D. Teaney, *Parton energy loss and momentum broadening at NLO in high temperature QCD plasmas*, *Int. J. Mod. Phys.* **E24** (2015) 1530013 [[1502.03730](#)].
- [21] J. Ghiglieri, J. Hong, A. Kurkela, E. Lu, G. D. Moore and D. Teaney, *Next-to-leading order thermal photon production in a weakly coupled quark-gluon plasma*, *JHEP* **1305** (2013) 010 [[1302.5970](#)].

- [22] J. Ghiglieri, G. D. Moore and D. Teaney, *QCD Shear Viscosity at (almost) NLO*, *JHEP* **03** (2018) 179 [[1802.09535](#)].
- [23] J. Ghiglieri, G. D. Moore and D. Teaney, *Second-order Hydrodynamics in Next-to-Leading-Order QCD*, *Phys. Rev. Lett.* **121** (2018) 052302 [[1805.02663](#)].
- [24] D. d’Enterria, *Jet quenching*, Springer Verlag, Landholt-Boernstein **Vol. 1-23A** (2009) [[0902.2011](#)].
- [25] U. A. Wiedemann, *Jet Quenching in Heavy Ion Collisions*, [0908.2306](#).
- [26] A. Majumder and M. Van Leeuwen, *The Theory and Phenomenology of Perturbative QCD Based Jet Quenching*, *Prog.Part.Nucl.Phys.* **A66** (2011) 41 [[1002.2206](#)].
- [27] Y. Mehtar-Tani, J. G. Milhano and K. Tywoniuk, *Jet physics in heavy-ion collisions*, *Int.J.Mod.Phys.* **A28** (2013) 1340013 [[1302.2579](#)].
- [28] G. Roland, K. Safarik and P. Steinberg, *Heavy-ion collisions at the LHC*, *Prog.Part.Nucl.Phys.* **77** (2014) 70.
- [29] G.-Y. Qin and X.-N. Wang, *Jet quenching in high-energy heavy-ion collisions*, *Int. J. Mod. Phys.* **E24** (2015) 1530014 [[1511.00790](#)].
- [30] M. Connors, C. Nattrass, R. Reed and S. Salur, *Jet measurements in heavy ion physics*, *Rev. Mod. Phys.* **90** (2018) 025005 [[1705.01974](#)].
- [31] JET collaboration, K. M. Burke et al., *Extracting the jet transport coefficient from jet quenching in high-energy heavy-ion collisions*, *Phys.Rev.* **C90** (2014) 014909 [[1312.5003](#)].
- [32] N. Armesto et al., *Comparison of Jet Quenching Formalisms for a Quark-Gluon Plasma ‘Brick’*, *Phys. Rev.* **C86** (2012) 064904 [[1106.1106](#)].
- [33] H. Liu, K. Rajagopal and U. A. Wiedemann, *Calculating the jet quenching parameter from AdS/CFT*, *Phys. Rev. Lett.* **97** (2006) 182301 [[hep-ph/0605178](#)].
- [34] H. Liu, K. Rajagopal and U. A. Wiedemann, *Wilson loops in heavy ion collisions and their calculation in AdS/CFT*, *JHEP* **03** (2007) 066 [[hep-ph/0612168](#)].
- [35] F. D’Eramo, H. Liu and K. Rajagopal, *Transverse Momentum Broadening and the Jet Quenching Parameter, Redux*, *Phys.Rev.* **D84** (2011) 065015 [[1006.1367](#)].
- [36] N. Armesto, J. D. Edelstein and J. Mas, *Jet quenching at finite ‘t Hooft coupling and chemical potential from AdS/CFT*, *JHEP* **09** (2006) 039 [[hep-ph/0606245](#)].
- [37] S. S. Gubser, *Momentum fluctuations of heavy quarks in the gauge-string duality*, *Nucl. Phys.* **B790** (2008) 175 [[hep-th/0612143](#)].
- [38] J. Casalderrey-Solana and D. Teaney, *Transverse Momentum Broadening of a Fast Quark in a  $N=4$  Yang Mills Plasma*, *JHEP* **04** (2007) 039 [[hep-th/0701123](#)].
- [39] P. Aurenche, F. Gelis and H. Zaraket, *A Simple sum rule for the thermal gluon spectral function and applications*, *JHEP* **0205** (2002) 043 [[hep-ph/0204146](#)].
- [40] P. B. Arnold and W. Xiao, *High-energy jet quenching in weakly-coupled quark-gluon plasmas*, *Phys.Rev.* **D78** (2008) 125008 [[0810.1026](#)].
- [41] P. B. Arnold, G. D. Moore and L. G. Yaffe, *Effective kinetic theory for high temperature gauge theories*, *JHEP* **0301** (2003) 030 [[hep-ph/0209353](#)].
- [42] J. Ghiglieri, G. D. Moore and D. Teaney, *Jet-Medium Interactions at NLO in a Weakly-Coupled Quark-Gluon Plasma*, *JHEP* **03** (2016) 095 [[1509.07773](#)].

- [43] M. Benzke, N. Brambilla, M. A. Escobedo and A. Vairo, *Gauge invariant definition of the jet quenching parameter*, *JHEP* **1302** (2013) 129 [[1208.4253](#)].
- [44] E. Braaten, *Solution to the perturbative infrared catastrophe of hot gauge theories*, *Phys.Rev.Lett.* **74** (1995) 2164 [[hep-ph/9409434](#)].
- [45] E. Braaten and A. Nieto, *Effective field theory approach to high temperature thermodynamics*, *Phys.Rev.* **D51** (1995) 6990 [[hep-ph/9501375](#)].
- [46] E. Braaten and A. Nieto, *Free energy of QCD at high temperature*, *Phys.Rev.* **D53** (1996) 3421 [[hep-ph/9510408](#)].
- [47] K. Kajantie, M. Laine, K. Rummukainen and M. E. Shaposhnikov, *Generic rules for high temperature dimensional reduction and their application to the standard model*, *Nucl.Phys.* **B458** (1996) 90 [[hep-ph/9508379](#)].
- [48] K. Kajantie, M. Laine, K. Rummukainen and M. E. Shaposhnikov, *3-D  $SU(N)$  + adjoint Higgs theory and finite temperature QCD*, *Nucl.Phys.* **B503** (1997) 357 [[hep-ph/9704416](#)].
- [49] A. Nieto and M. H. G. Tytgat, *Effective field theory approach to  $\mathcal{N} = 4$  supersymmetric Yang-Mills at finite temperature*, [hep-th/9906147](#).
- [50] M. A. Vazquez-Mozo, *A Note on supersymmetric Yang-Mills thermodynamics*, *Phys. Rev.* **D60** (1999) 106010 [[hep-th/9905030](#)].
- [51] C.-j. Kim and S.-J. Rey, *Thermodynamics of large  $N$  superYang-Mills theory and AdS / CFT correspondence*, *Nucl. Phys.* **B564** (2000) 430 [[hep-th/9905205](#)].
- [52] A. Anisimov, D. Besak and D. Bodeker, *Thermal production of relativistic Majorana neutrinos: Strong enhancement by multiple soft scattering*, *JCAP* **1103** (2011) 042 [[1012.3784](#)].
- [53] D. Besak and D. Bödeker, *Thermal production of ultrarelativistic right-handed neutrinos: Complete leading-order results*, *JCAP* **1203** (2012) 029 [[1202.1288](#)].
- [54] J. Ghiglieri and M. Laine, *Neutrino dynamics below the electroweak crossover*, *JCAP* **1607** (2016) 015 [[1605.07720](#)].
- [55] F. D’Eramo, M. Lekaveckas, H. Liu and K. Rajagopal, *Momentum Broadening in Weakly Coupled Quark-Gluon Plasma (with a view to finding the quasiparticles within liquid quark-gluon plasma)*, *JHEP* **05** (2013) 031 [[1211.1922](#)].
- [56] A. D. Linde, *Infrared Problem in Thermodynamics of the Yang-Mills Gas*, *Phys.Lett.* **B96** (1980) 289.
- [57] M. Laine, *A non-perturbative contribution to jet quenching*, *Eur.Phys.J.* **C72** (2012) 2233 [[1208.5707](#)].
- [58] M. Panero, K. Rummukainen and A. Schäfer, *A lattice study of the jet quenching parameter*, *Phys.Rev.Lett.* **112** (2014) 162001 [[1307.5850](#)].
- [59] E. Braaten and R. D. Pisarski, *Soft Amplitudes in Hot Gauge Theories: A General Analysis*, *Nucl.Phys.* **B337** (1990) 569.
- [60] J. Frenkel and J. Taylor, *High Temperature Limit of Thermal QCD*, *Nucl.Phys.* **B334** (1990) 199.
- [61] A. Czajka and S. Mrowczynski,  *$N=4$  Super Yang-Mills Plasma*, *Phys. Rev.* **D86** (2012) 025017 [[1203.1856](#)].

- [62] S. Caron-Huot, *On supersymmetry at finite temperature*, *Phys.Rev.* **D79** (2009) 125002 [[0808.0155](#)].
- [63] P. B. Arnold, G. D. Moore and L. G. Yaffe, *Photon and gluon emission in relativistic plasmas*, *JHEP* **0206** (2002) 030 [[hep-ph/0204343](#)].
- [64] S. Jeon and G. D. Moore, *Energy loss of leading partons in a thermal QCD medium*, *Phys.Rev.* **C71** (2005) 034901 [[hep-ph/0309332](#)].
- [65] G. Moliere, *Theorie der Streuung schneller geladener Teilchen I. Einzelstreuung am abgeschirmten Coulomb-Feld*, *Z. Naturforsch.* **A2** (1947) 133.
- [66] G. Moliere, *Theory of the scattering of fast charged particles. 2. Repeated and multiple scattering*, *Z. Naturforsch.* **A3** (1948) 78.
- [67] S. S. Gubser, I. R. Klebanov and A. A. Tseytlin, *Coupling constant dependence in the thermodynamics of  $N=4$  supersymmetric Yang-Mills theory*, *Nucl. Phys.* **B534** (1998) 202 [[hep-th/9805156](#)].
- [68] S. Borsanyi, Z. Fodor, C. Hoelbling, S. D. Katz, S. Krieg and K. K. Szabo, *Full result for the QCD equation of state with 2+1 flavors*, *Phys. Lett.* **B730** (2014) 99 [[1309.5258](#)].
- [69] HOTQCD collaboration, A. Bazavov et al., *Equation of state in (2+1)-flavor QCD*, *Phys. Rev.* **D90** (2014) 094503 [[1407.6387](#)].
- [70] F. D’Eramo, K. Rajagopal and Y. Yin, *Molière Scattering in Quark-Gluon Plasma: Finding Point-Like Scatterers in a Liquid*, [1808.03250](#).
- [71] P. B. Arnold, G. D. Moore and L. G. Yaffe, *Photon emission from ultrarelativistic plasmas*, *JHEP* **0111** (2001) 057 [[hep-ph/0109064](#)].
- [72] P. Aurenche, F. Gelis, G. Moore and H. Zaraket, *Landau-Pomeranchuk-Migdal resummation for dilepton production*, *JHEP* **0212** (2002) 006 [[hep-ph/0211036](#)].
- [73] S. Catterall, D. B. Kaplan and M. Unsal, *Exact lattice supersymmetry*, *Phys. Rept.* **484** (2009) 71 [[0903.4881](#)].
- [74] G. Bergner and S. Catterall, *Supersymmetry on the lattice*, *Int. J. Mod. Phys.* **A31** (2016) 1643005 [[1603.04478](#)].